On the intimate connection between nanoscale adhesion of Yad fimbriae and macroscale attachment of Yad-decorated bacteria to glycosylated, hydrophobic and hydrophilic surfaces.

Gregory Francius, Florian Petit, Eloïse Clément, Yankel Chekli, Jean-Marc Ghigo, Christophe Beloin, Jérôme D.F. Duval

View Article Online
DOI: 10.1039/D0NR06840C

On the intimate connection between nanoscale adhesion of Yad fimbriae and macroscale attachment of Yad-decorated bacteria to glycosylated, hydrophobic and hydrophilic surfaces

Grégory Francius[1*], Florian Petit[1], Eloïse Clément[1], Yankel Chekli[2,3], Jean-Marc Ghigo[2], Christophe Beloin[2,#], Jérôme F.L. Duval[4,#]

[1] Université de Lorraine, LCPME, UMR 7564, Villers-lès-Nancy, F-54600, France.

[2] Genetics of Biofilms Laboratory, Institut Pasteur, UMR CNRS2001, Paris, 75015, France.

[3] Université de Paris, Sorbonne Paris Cité, Paris, France.

[4] Université de Lorraine, LIEC, UMR 7360, Vandœuvre-lès-Nancy, F-54501, France.

equivalent contribution

* Corresponding authors:

gregory.francius@univ-lorraine.fr

View Article Online
DOI: 10.1039/D0NR06840C

Abstract

Yad fimbriae are currently viewed as versatile bacterial adhesins able to significantly mediate host or plant-pathogen recognition and contribute to the persistence of *Escherichia coli* in both the environment and within hosts. To date, however, the underlying adhesion process of Yad fimbriae on surfaces defined by controlled coating chemistries have not been evaluated at the relevant molecular scale. In this work, the interaction forces operational between Yad fimbriae expressed by genetically modified *E. coli* and self-assembled monolayers (SAM) differing in terms of charge, hydrophobicity or nature of decorating sugar units, are quantified by Single Molecule Force Spectroscopy (SMFS) at the nanoscale. It is found that the adhesion of Yad fimbriae onto probes functionalized with xylose is as strong as that measured with probes decorated by anti-Yad antibodies (*ca*. 80 to 300 pN). In contrast, the interactions of Yad with galactose, lactose, mannose, -OH, $-NH_2$, -COOH and $-CH_3$ terminated-SAMs are clearly non-specific. Interpretation of SMFS measurements on the basis of Worm-Like-Chain modeling for polypeptide nanomechanics further leads to estimate of the maximal extension of Yad fimbriae upon stretching, that of their persistence length and of their polydispersity. Finally, we evidence for the first time a strong correlation between the adhesion properties of Yad-decorated bacteria addressed from conventional macroscopic counting methods, and the molecular adhesion capacity of Yad fimbriae. Such demonstration advocates for the effort that should be made to understand at the nanoscale level the interactions between fimbriae and their cognate ligands. The results could further help the design of potential anti-adhesive molecules or surfaces to better fight against the virulence of bacterial pathogens.

Keywords:

Single molecule force spectroscopy, bacterial adhesion, Yad fimbriae, glycosylated surfaces, Atomic Force Microscopy.

View Article Online
DOI: 10.1039/D0NR06840C

Introduction

Bacterial adhesion and biofilm formation onto biotic and abiotic surfaces are ubiquitous processes that contribute to the adaptation and living of bacteria even under extreme environmental conditions. Since pathogenic bacteria can form biofilms, these processes have become an issue of societal concern and a major challenge in various scientific and applied fields, especially in food and medical industries.[1-5] For illustration, the ability of some bacteria to adhere onto the surface of fruits or vegetables represents a possible source of foodborne illness and global epidemic outbreak.[6-9]

One of the most recent food-linked outbreak occurred in 2011, when a bacterial epidemics related to enterohemorrhagic *Escherichia coli* (EHEC) strains developed in Germany, then spread to several adjacent countries and ended in a health crisis at the European level.[10, 11] This epidemic mainly affected children, causing mucous-bloody diarrhea, hemolytic and uremic syndromes, and caused the death of hundreds of people all over Europe.[12] Epidemiological studies evidenced that the lethal infections were caused by an EHEC strain O104:H4[10, 11] and they hypothesized that the epidemic followed the consumption of contaminated fresh vegetables.[12] These virulent *E. coli* strains belong to a rare serotype defined by its ability to produce shigatoxin (STEC)[13, 14] and by its facilitated propensity to adhere to digestive mucosa.[15] This specific epidemic case pinpointed the importance of adhesion and colonization factors in the success of a pathogen spread.

Several studies have demonstrated that bacterial adhesion in the digestive tract is mediated by specific fimbriae or pili located at the bacterial surface.[16, 17] These fimbriae serve as anchoring bridges to the neighboring environment of the cells and they further contribute to the aggregative adhesion of so-called enteroaggregative *E. coli* (EAEC) strains.[15, 18, 19] Some of these fimbriae are also known to enhance the virulence of extra-intestinal *E. coli* (EXPEC) strains.[20-22] Given these contextual elements, much work has focused on the identification and

View Article Online
DOI: 10.1039/D0NR06840C

characterization of fimbriae composition and structure, as well as on the understanding of their role in adhesion and virulence. Such knowledge is further mandatory for the elaboration of efficient strategies aimed at killing *e.g.* antibiotic resistant cells or at suppressing the adhesion of *e.g.* pathogenic bacteria to surfaces and thereby preventing epidemic risks related to *e.g*. food poisoning.[23, 24] In that respect, deciphering at the molecular scale the role of fimbriae and of the adhesins positioned at their extremities is urgently needed to address the mechanisms underlying the biomolecular recognition of biotic surfaces and ensuing virulence pattern.

Among the so-called chaperone usher family of fimbriae,[25, 26] the Yad fimbriae are amongst the most prevalent and conserved fimbriae in *E. coli* [27] and were demonstrated to modulate bacterial adhesion, biofilm formation and macrophage phagocytosis of different types of *E. coli*.[28, 29] The Yad fimbriae are composed mostly of YadN major pilin sub-units forming the fimbrial shaft, YadM, YadL, YadK minor pilins and the YadC adhesin displayed at the tip of the fimbriae.[30] The YadC adhesin is a lectin known for its affinity to xylose[30] and for its role in the colonization of corn seed rhizospheres by bacteria.[30] D-xylose is obtained from hemicellulose and it is generally found in the composition of leaves and bark of plants but also at the surface of some fruits and vegetables.[31-33] As *E. coli* including EHEC and UPEC strains can bind to- and form biofilms onto- plants and animal cells, their resistance/tolerance to antibiotic treatments further represents a challenge for the development of non-antibiotic-based therapies.[34-36] Interestingly, the use of anti-adhesive agents such as globotetraose for P pili or mannosides for type 1 fimbriae is very performant to inhibit bacterial adhesion.[37, 38] There is therefore much to gain in better understanding how these fimbriae interact with their cognate sugar, and to date, quantitative information on the interaction of Yad fimbriae with xylose remains limited.

The purpose of the current work is to address the adhesion of Yad fimbriae-decorated bacteria onto several self-assembled monolayers with various terminal groups (-OH, -CH_3, -COOH, -NH_2) or conjugated to different sugar molecules (D-xylose, D-galactose, D-mannose and D-

View Article Online
DOI: 10.1039/D0NR06840C

lactose), both at the molecular and bacterial population scales. The molecular adhesion of Yad fimbriae to sugar molecules is here retrieved by atomic force spectroscopy operated at the single molecule level (Single Molecule Force Spectroscopy, SMFS for short) with use of dedicated anti-Yad functionalized probe, whereas macroscopic cell adhesion behavior is evaluated by conventional fluorescence-based counting method. The objectives are to i) evidence the existence (or not) of a clear recognition between Yad fimbriae and several model glycosurfaces with controlled surface chemistries, ii) quantify the magnitude of the corresponding molecular interactions forces, and iii) analyze the molecular Yad adhesion features in relation to the macroscopic bacterial adhesion properties. For the sake of comparison, all results pertaining to the adhesion properties of Yad fimbriae and Yad fimbriae-decorated bacteria with respect to sugars and corresponding glycosylated surfaces are systematically set against those obtained from the molecular interactions measured between functionalized AFM probes and macrosurfaces decorated by antibodies that specifically target the YadC and YadN sub-units of the Yad fimbriae. The results allow a classification of the magnitude of the interaction force operational between Yad fimbriae and various surfaces differing in terms of hydrophilic/hydrophobic balance and nature of the sugar units they support. The analysis further unequivocally demonstrates that macroscopic adhesion of Yad-decorated bacteria is dictated by the very molecular adhesion properties of the Yad fimbriae.

Materials and methods

Bacterial strains

The genetic profiles of two *E. coli* K-12 mutant strains used in this study (Δ_4*adh* and Δ_4*adh*_PcL*yad*) are summarized in **Table 1**. They derived from previously constructed strains.[30, 39] The isogenic Δ_4*adh*_PcL*yad* and Δ_4*adh* strains, producing or not Yad fimbriae, respectively, were constructed from *E. coli* MG1655 (*E. coli* genetic stock center CGSC#6300).

They carry the *gfpmut3* gene, encoding the Gfp protein, linked to the *bla* ampicillin resistance gene (*amp*^{R}, 100 µg/mL) as well as a deletion of the *fliE* to *fliR* flagellar genes replaced by the *cat* chloramphenicol resistance gene (*cm*^{R}, 25 µg/mL). Both strains have been additionally deleted for the *fim* operon encoding type 1 fimbriae (Δ*fimA-H*::*zeo, zeo*^{R} 50 µg/mL), for the *agn43* gene, encoding the Ag43 auto-aggregating protein, with the Kanamycin resistance encoding gene that has been flipped out using the pCP20 plasmid (Δ*flu*::FRT)[40] as well as for the *csgA* gene encoding the main component of the curli fimbriae. These two strains are then deleted for the four main adhesins/cell surface appendages of *E. coli* K-12. In *E. coli* K-12, the *yad* fimbrial operon is cryptic.[30, 41] Then, to evaluate the impact of the production of the Yad fimbriae, we additionally transduced the *km*PcL*yad* construction into the Δ_4*adh* strain to obtain the Δ_4*adh*_PcL*yad* strain. In this latter strain, the *yad* operon is under control of the lambda P_R promoter and is expressed constitutively.

Bacterial growth conditions, and sample preparation for Atomic Force Microscopy (AFM) imaging.

Bacteria were pre-grown overnight at 30°C without agitation in M63B1 minimal medium supplemented with 0.4% glucose (M63B1glu) and with the appropriate antibiotics for the proper selection of the strain of interest (**Table 1**). The next day, fresh M63B1glu medium was inoculated with the overnight culture (OD_{600} of *ca.* 0.05) and cultivated under the same conditions until the biomass reached an OD_{600} of 0.5. Then, 200 µL of the bacterial suspension were placed onto NH_2-decorated substrates for 30 minutes, as detailed in the next section. The samples were extensively rinsed with PBS solution to remove M63B1glu, and placed directly into the AFM closed fluid-cell with 2 mL PBS solution.

Preparation of Yad antibodies-decorated surfaces, self-assembled monolayers and

View Article Online
DOI: 10.1039/D0NR06840C

glycosylated surfaces

Rabbit polyclonal antibodies against *E. coli* YadC and YadN proteins were generated previously[30] and absorbed on whole protein lysates of MG1655_Δ*yad* strain. IgG were then purified and concentrated using the NAb Protein A/G Spin Purification Kit (Thermo Fisher Scientific) and dialyzed against PBS using Slide-A-Lyzer® MINI Dialysis Devices, 10 K MWCO, 0.5 mL (Thermo Fisher Scientific). D-Mannosamine ($C_6H_{11}O_5$-NH_2), ethanolamine (C_2H_7NO), dimethylsulfoxyde (DMSO), triethylamine ($C_6H_{15}N$), sodium cyanoborohydride ($NaCNBH_3$), N-(3-Dimethylaminopropyl)-N′-ethylcarbodiimide hydrochloride (EDC), N-hydroxysuccinimide (NHS), 1-dodecanethiols (HS-$C_{11}H_{22}$-CH_3), 11-Amino-1-undecanethiol hydrochloride (HS-$C_{11}H_{22}$-NH_2), 12-mercapto-1-undecanoic acid (HS-$C_{11}H_{22}$-COOH), 11-Mercapto-1-undecanol (HS-$C_{11}H_{22}$-OH) and PBS tabs were purchased from Sigma-Aldrich (Sigma Aldrich, Saint-Quentin Fallavier, France) and used as received. PEG-acetal linkers were purchased from Hermann Gruber group (Institute of Biophysics, University of Linz, Austria). Gold-coated glass substrates were obtained by means of a sputter coater (Milexia, K575 Turbo Q150T S, France). In detail, the borosilicate substrates (ref. OVM4-0.9514 of 14 mm ×14 mm ×1 mm) were purchased from Preciver (Preciver Activités, Noisy-le-Grand, France) and were coated with a 20 nm thick chromium layer and a topmost 60 nm gold layer. Gold-coated glass slides were subsequently cleaned with chloroform for 10 min, dried with nitrogen, and then placed into a UV-ozone cleaner (PSD UV4, Novascan Technologies Inc. Ames, IA) for 30 min. Substrates with -NH_2, -OH, -CH_3 and -COOH as terminal groups were prepared according to the following procedure. One side of the gold-coated glass slides previously prepared were brought overnight in contact with a solution of alkanethiols (either HS-$C_{11}H_{22}$-NH_2, HS-$C_{11}H_{22}$-OH, HS-$C_{11}H_{22}$-CH_3 or HS-$C_{11}H_{22}$-COOH) at 1 mM in pure ethanol. Samples were then abundantly rinsed twice with ethanol for 10 min, dried with nitrogen beam and stored in PBS solution at 4°C prior to experiments.

Prior to the preparation of the different antibodies and of the glycosylated surfaces of interest in this work, one side of the gold-coated glass slides was brought overnight in contact with a 1 mM solution of (HS-$C_{11}H_{22}$-COOH) with pure ethanol as solvent. Samples were then extensively rinsed, twice, with ethanol for 10 min, dried with nitrogen beam and brought in contact for 30 minutes with a solution of EDC/NHS (50 mg/mL: 20 mg/mL) dissolved in water at pH 5.0 in order to activate the carboxylic sites of the substrates. Then, the samples were directly immersed into a solution containing the amino-sugar (either antibodies, xylosamine (Xyl), mannosamine (Man), galactosamine (Gal), lactosamine (Lac)) dissolved at 1 mg/mL in PBS at pH 5.0 for 2 hours. At the end of this step, substrates were dipped in a PBS solution at pH 8.0 for 10 minutes, and extensively rinsed with milli-Q water, and finally stored in PBS solution at 4°C.

Infrared reflection absorption spectroscopy (IRRAS)

IRRAS spectra were recorded in the mid-infrared range with use of a Fourier transform infrared spectrometer Nicolet 8700 apparatus equipped with a KBr beam splitter and a MCT detector. An advanced grazing angle specular reflectance accessory (Pike technologies Inc.) with a fixed incidence angle of 80° was used to acquire spectra of the gold-coated surfaces. The spectral resolution was 4 cm^{-1} and the accumulation time was 2 min. Compartments containing the detector and the specular reflectance accessory were purged by circulating dry N_2. IR absorbance spectra were obtained between 4000 and 600 cm^{-1}. Note that samples were extensively rinsed with milli-Q water and then dried with dry N_2 *prior* to measurement and introduction in the spectrophotometer. A total of 200 scans were collected for each sample and condition examined.

Bacterial adhesion by fluorescence microscopy and bacterial membrane integrity assays.

Bacterial adhesion was determined by counting GFP positive Δ_4*adh* and Δ_4*adh* PcI*yad* bacteria attached to the functionalized surfaces. Briefly, 1 mL of OD_{600} 0.5 cells were deposited on the different functionalized substrates and left for 2h. Bacterial membrane integrity was assessed with propidium iodide (PI) at 160 µM concentration in sterile PBS. This allows assessing the toxicity of the tested surface coatings against the cells since PI enters the cells only when their membranes are damaged. The bacteria adhered onto the different functionalized substrates were stained with PI during 20 minutes under dark conditions. Then, the samples were rinsed with sterile PBS buffer solution (pH 7.4) to eliminate the excess of dyes, and then fixed with a solution of glutaraldehyde at 2% in PBS for 30 minutes. Subsequently, samples were set in mounting oil environment. Sets of 10 images per samples with green and red fluorescence emissions were acquired simultaneously with the × 100 oil immersion objective of an Olympus BX51 microscope equipped with an Olympus XC50 camera. PI and GFP fluorescence were observed simultaneously using fluorescence filter cube U-MWIB3 (Olympus, excitation filter: BP 460-495 nm, emission filter: LP 510 nm).

AFM-probes functionalization.

AFM-probes were functionalized with amino-sugars (xylosamine (Xyl), mannosamine (Man), galactosamine (Gal), lactosamine (Lac)), anti-YadC or anti-YadN antibodies according to the procedure described elsewhere[42-44] and successfully adopted for the detection and stretching of type 1 fimbriae.[45] Briefly, silicon nitride tips (MLCT, Bruker Nano AXS, Palaiseau, France, spring constant of about 0.01 nN/nm) were first amino-functionalized according to the protocol detailed elsewhere[46] and tips modified with amino groups further reacted with PEG linkers carrying benzaldehyde functions. The latter were then directly attached to the amino-sugars or antibodies through their terminal NH_2 group.

View Article Online
DOI: 10.1039/D0NR06840C

AFM imaging and single-molecule force spectroscopy (SMFS)

AFM images were recorded with a Bioscope Resolve equipment (Bruker AXS, Palaiseau, France) using PeakForce Tapping mode[47, 48] to image the biological surfaces of interest under air conditions. Force measurements were carried out with a MFP3D-BIO instrument (Oxford Instruments, Mannheim, Germany). Silicon nitride and gold coated cantilevers of conical shape were purchased from Bruker (MLCT and NPG, Bruker AXS, Palaiseau, France) with spring constants of 0.01 nN/nm and 0.12 nN/nm, respectively. Single molecule force spectroscopy experiments were performed in PBS at pH 7.4 and room temperature.

Adhesion forces, conformational characteristics and extension of the Yad fimbriae were measured by recording Force-Volume Images (FVI) consisting of a grid of 32 × 32 force curves obtained upon approach and subsequent retraction of the chemically-modified AFM probe at pulling rates of 1 µm/s (SMFS experiments). For each condition examined, force measurements were performed in triplicate over an area of 5 µm × 5 µm after locating the selected bacteria *via* the Olympus IX 71 inverted microscope that supports the AFM.

During SMFS experiments, the Yad fimbriae were detected and stretched upon withdrawal of the chemically-modified AFM probe away from the surface. The obtained force-distance curves were then analyzed on the basis of the Worm Like Chain (WLC) model.[45, 49] This model is most suitable and most frequently used to describe the extension of polypeptides. Within the framework of this theory, the extension z of the macromolecule is related to the retraction force F_{adh} *via* the following equation:[50, 51]

$$F_{\mathrm{adh}}(z) = -\frac{k_B T}{l_p}\left[\frac{z}{L_c} + 4\left(1 - \frac{z}{L_c}\right)^{-2} - \frac{1}{4}\right] \quad (1)$$

where the persistence length l_p reflects chain stiffness, L_c is the total contour length of the macromolecule and k_B is the Boltzmann constant. All FVI were analyzed automatically with

use of a home-made MATLAB program described elsewhere.[49] It is emphasized that force-distance curve measurements were systematically performed on freshly prepared substrates.

Results and discussion

Morphological analysis of bacteria constitutively expressing Yad fimbriae

To gain insight into the cell surface morphology of *E. coli* K-12 producing Yad fimbriae, the strains Δ_4*adh* and Yad fimbriae-producing Δ_4*adh*_PcL*yad* were grown at 30°C without any agitation prior to electrostatic immobilization onto a gold substrate exhibiting -NH_2 terminal groups, and then gently dehydrated before imaging by AFM (**Figure 1** and **Figure S1** in **Supporting Information**). AFM images clearly showed that Δ_4*adh*_PcL*yad* bacteria constitutively expressing Yad fimbriae are 2.0-2.5 µm rod-like shaped cells decorated with several 50 to 2000 nm long filamentous structures. In contrast, the Δ_4*adh* bacteria are devoid of such peripheral structures (**Figures 1-S1)**. Accordingly, these filamentous structures should correspond to the Yad fimbriae with a typical tubular structure of about 1-2 µm length and 5-8 nm in diameter as roughly determined from horizontal cross-sections profiling. This is consistent with previous observation of Yad fimbriae using transmission electron microscopy.[30] The thin Yad fimbriae are fragile structures, as judged by the presence of many bundles of broken filaments at the substrate surface (**Figure 1**). These broken fimbriae exhibit an average length ranging from *ca.* 50 nm to 1000 nm and are randomly distributed around individual bacterium. These observations related to the fragility of Yad fimbriae are probably the result of structure cracking during the required rinsing step of the sample. Due to the inherent dynamics of fimbriae structures and technical limitation of the used AFM, Yad filaments could not be observed in liquid medium.

IRRAS analysis of the model self-assembled monolayers terminated with -NH_2, -OH, -CH_3, -COOH, anti-Yad antibodies or sugars (mannose, lactose, galactose and xylose)

Prior to investigation of the impact of chemical coatings on the adhesion properties of Δ_4*adh* and Δ_4*adh*_PcL*yad* cells, the surface chemistry of the different self-assembled monolayers formed onto the gold-coated substrates was verified by IRRAS (**Figure S2**). The IRRAS spectra of the model substrates obtained by simple adsorption of HS-$C_{11}H_{22}$-NH_2 (SAM-NH_2), HS-$C_{11}H_{22}$-OH (SAM-OH), HS-$C_{11}H_{22}$-CH_3 (SAM-CH_3) and HS-$C_{11}H_{22}$-COOH (SAM-COOH) show typical absorption bands from the alkyl chain identified at 2950, 2922, 2850, 1450 and 1065 cm^{-1}, respectively for the C-H and C-C bonds. The different terminal groups were clearly evidenced by the typical absorption bands at 3395, 3250 and 1550 cm^{-1} for -NH_2, at 3500 and 1080 cm^{-1} for -OH, and at 17450 cm^{-1} for -COOH.

Concerning the glycosurfaces of interest in this work (SAM-Xylose, SAM-Mannose, SAM-Galactose and SAM-Lactose), their corresponding IRRAS spectra (**Figure S2**) show absorption bands from mannosylated residue at 1510, 1425, 1342, 1267 and 1083 cm^{-1}, from lactosyl at 1435, 1382, 1265, 1163 and 1077 cm^{-1}, from galactosyl at 1571, 1470, 1388, 1218 and 1161 cm^{-1} and from xylosyl at 1461, 1365, 1314, 1282 and 1081 cm^{-1}.[52, 53] The IRRAS spectra of substrates covered by a monolayer of anti-YadC and anti-YadN antibodies feature absorption bands of the proteins at 1653, 1546, 1745 and 1269 cm^{-1}, respectively assigned to amide I, amide II bands, ester groups (C=O) and ν(C-N) bond. Altogether, the chemical surface analyses confirmed the presence of controlled molecular monolayers at the surface of the different gold substrates and, consequently, they support the success of the functionalization procedure we followed.

Influence of the substrate chemistry on the macroscopic adhesion of *E. coli* cells producing or not the Yad fimbriae.

In order to evaluate how the surface chemistry of the various self-assembled monolayers (SAM) determine bacterial adhesion, we incubated the different substrates with defining IRRAS spectra given in **Figure S2** in suspension of GFP fluorescent *E. coli* Δ_4*adh* and Δ_4*adh*_PcL*yad* cells during 2 hours. Then, after rinsing, samples were stained with the propidium iodide viability dye to assess the toxicity of the functionalized surfaces. Adhered bacteria onto the different substrates were counted upon analysis of attached GFP+ bacterial cells (**Figure 2a**). For the sake of completeness, **Figure S3** and **Figure S4** report characteristic epifluorescence images recorded for the two *E. coli* strains on the surface of the various substrates selected in this work. None of the surface appeared to display any significant toxicity as shown by the absence of, or low level of PI red fluorescence of the cells attached to the different surfaces (**Figure S3** and **Figure S4**). Consistently with the fact that, unlike Δ_4*adh* cells, the Δ_4*adh*_PcL*yad* cells produce the Yad fimbriae, the results evidence that the amount of Δ_4*adh*_PcL*yad* cells adhered at the substrates covered by the anti-YadC and anti-YadN antibodies is significantly higher, by *ca.* three orders of magnitude, than that for Δ_4*adh* cells. In detail, the estimated surface concentrations of adhered Δ_4*adh* and Δ_4*adh*_PcL*yad* are 4-5×10^4 and 2-4×10^7 cells/cm^2, respectively, for the anti-YadC and anti-YadN substrates. A similar result is obtained regarding the amount of adhered Δ_4*adh* and Δ_4*adh*_PcL*yad* cells onto the glycosubstrate with xylose (Xyl) coating, with surface concentrations of adhered Δ_4*adh* and Δ_4*adh*_PcL*yad* of *ca.* (5.4±1.3)×10^4 and (2.4±0.7)×10^7 cells/cm^2, respectively. This finding is consistent with the specific binding of the YadC tip adhesin to xylose.[30] Results pertaining to the adhesion of Δ_4*adh* and Δ_4*adh*_PcL*yad* cells onto the glycosubstrates with Galactose (Gal), Mannose (Man) and Lactose (Lac) coatings reveal that, here again, cells expressing Yad fimbriae exhibit stronger adhesion properties, *albeit* with a difference for these 3 glycosubstrates that is far lesser marked than that discussed for surfaces covered by anti-Yad antibodies and Xylose. Quantitatively, the ratio Δ_4*adh*_PcL*yad* and Δ_4*adh* cells surface

concentrations now amounts to *ca.* 2-4 on SAM-Gal, SAM-Man and SAM-Lac, to be compared with the 650-1000 ratio for substrates covered with Xyl or anti-Yad antibodies.

Adhesion of *E. coli* Δ_4*adh* and Δ_4*adh*_PcL*yad* cells on substrates covered by self-assembled monolayers (SAM) terminated by -NH_2, -COOH, -OH and -CH_3 groups was also evaluated in order to address the impact of surface charge and hydrophilic/hydrophobic balance on cell adhesion features. A detailed analysis of the electrostatic features of the substrates adopted in this work could be performed on the basis of streaming-potential/current measurements and proper interpretation thereof with inclusion of ionic surface conduction if relevant,[54] or on the basis of chemical force spectroscopy data.[55] Within the scope of the current work, it is sufficient to state that given the typical dissociation properties of carboxylic and amine groups and considering the pH condition of interest for our SMFS measurements, the surface charge of SAM-NH_2 and SAM-COOH is positive and negative at pH 7.4, respectively, while SAM-OH and SAM-CH_3 groups are known to be hydrophilic and hydrophobic surfaces, respectively. The results for SAM-OH substrates (**Figure 2a**) indicate that surface of Δ_4*adh*_PcL*yad* cells is much more hydrophilic than that of Δ_4*adh* cells (surface concentrations of $(1.8\pm0.4)\times10^6$ and $(6.1\pm2.2)\times10^4$ cells/cm^2, respectively), which is confirmed by the data collected on SAM-CH_3 evidencing a Δ_4*adh*_PcL*yad* cells surface hydrophobicity that is significantly lower than for Δ_4*adh* cells (surface concentrations of $(6.1\pm2.2)\times10^4$ and $(1.1\pm0.3)\times10^6$ cells/cm^2, respectively). Analysis of cell adhesion onto SAM-NH_2 and SAM-COOH substrates further highlights that the affinity of Δ_4*adh* cells for positively charged surfaces is *ca.* 10 times higher than that of Δ_4*adh*_PcL*yad* cells, whereas both cells exhibit similar adhesion properties onto negatively charged substrate (SAM-COOH). Last, the affinity of Δ_4*adh* and Δ_4*adh*_PcL*yad* cells for positively charged surfaces is significantly higher (by a factor of *ca.* 20) than that for negatively charged substrates, in agreement with the sign of bacterial surface charge and the well-documented role of electrostatics on cell adhesion.[56, 57] The results detailed above are converted

into percentage of surface coverage by the bacteria (**Figure 2b**), which offers another representation of the respective adhesion properties of Δ_4*adh* and Δ_4*adh*_PcL*yad* cells discussed above for the various substrates considered in this work. For the surface coverage computation, the required uncovered surface area was evaluated with use of standard image-analysis procedure implemented in MATLAB™. Between 24% and 43% of the total initial amount of Δ_4*adh*_PcL*yad* bacteria could adhere onto the substrates covered by Xyl and antibodies, which corresponds to only 5-15% surface coverage. As far as the glycosubstrates and the other SAM-OH, SAM-NH_2, SAM-CH_3 and SAM-COOH surfaces are concerned, less than 1% of the total amount of initially incubated Δ_4*adh*_PcL*yad* bacteria adhered on the surface substrate, which amounts a surface coverage of less than 0.5%. These results clearly demonstrate a high affinity of Δ_4*adh*_PcL*yad* cells to substrates covered with Xyl or antibodies. Conversely, less than 3% of the total initial amount of Δ_4*adh* bacteria could adhere onto the substrate regardless of their surface chemistry, with a corresponding surface coverage lower than 0.5%. Altogether, our results clearly confirm that the adhesion of Δ_4*adh*_PcL*yad* to surfaces functionalized with Xyl and anti-Yad antibodies is specific and mediated by the Yad fimbriae. The developments below provide a molecular insight into this specificity of the interactions between Yad fimbriae and Xyl (or antibodies).

Deciphering the interactions between Yad fimbriae, antibodies and glycosyl residues at the molecular scale.

We performed single-molecule force spectroscopy measurements (SMFS) on Yad fimbriae exposed at the cell surface of living cells in order to quantify the interaction forces of Yad fimbriae with the glycosyl residues (Xyl, Man, Gal, Lac) or with the specific polyclonal antibodies (anti-YadC and anti-YadN). The latter allow the detection and specific targeting of YadC and YadN pilin constituting the tubular structure of the Yad fimbriae, with YadN being

View Article Online
DOI: 10.1039/D0NR06840C

the main constituent of the Yad filamentous structure and YadC being the adhesin located at the tip of the Yad fimbriae. Typical force curves recorded on Δ_4*adh*_PcL*yad* and Δ_4*adh* bacteria with the different functionalized AFM-probes are reported in **Figure 3** and **Figure S5**, respectively.

Unlike typical force curves reported in literature for several types of fimbriae (*e.g*. type 1, F1C, type 3, CFA/I), those obtained for Yad fimbriae are not defined by the succession of regimes that feature a plateau where the force remains constant upon increasing the separation distance between the AFM and the (elongated) structure.[45, 58-60] The presence of such a plateau for type 1 fimbriae is the signature of a tensed helical structure where the FimA sub-units conserve their conformation.[45, 61] Here, SMFS measurements do not reveal the occurrence of force plateau regime(s) but, instead, they evidence abrupt rupture events between segments of the Yad fimbriae structure and the molecules grafted on the AFM probe, as reflected by the discrete and successive drops of the force with pulling on Yad fimbriae. These findings demonstrate that the YadN sub-units constituting the helical structure of the Yad fimbriae do not retain their conformation when withdrawing the AFM probe from the cell wall but, instead, they are unfolded concomitantly to the stretching of the overall Yad fimbrial structure.

Starting the discussion with Δ_4*adh*_PcL*yad* cells, it is found that 87% to 98% of the force curves recorded with use of AFM-probes functionalized by anti-YadC, anti-YadN and Xyl exhibits at least one adhesive event. This finding contrasts with the 15% to 23% of the force curves for which at least one adhesive event is detected between Yad fimbriae and AFM-probe with the glycosyl functionalities Man, Gal and Lac (**Table 2**). Conversely, less than 5% of the force curves collected between Δ_4*adh* cells surface and AFM-probe contains the signature of -at least- one adhesive event and this conclusion holds for all probe functionalities tested, which includes the AFM- tip modified with YadC- and YadN- antibodies (see **Table 3)**. Stated differently, the cell wall of Δ_4*adh* cells interacts poorly with the various molecules grafted at the apex of the

View Article Online
DOI: 10.1039/D0NR06840C

AFM-probes. Unlike Δ_4*adh* cells, a significant number of interactions take place between the bacterial cell wall of Δ_4*adh*_PcL*yad* cells and the different molecules grafted at the end of the AFM-probes, especially Xyl and, obviously, anti-Yad antibodies. These interactions should therefore be attributed to Yad fimbriae. The occurrence of weak interactions between Δ_4*adh*_PcL*yad* cells with the substrates covered by sugar molecules other than xylose or by the functional groups -OH, -NH_2, -CH_3 and -COOH could originate from non-specific interactions. Indeed, other sub-units of the Yad fimbriae (YadK, YadL, YadM and YadN) could interact in a non-specific manner with these functional groups leading to a weak but measurable adhesion. This result has been already reported for type 1 fimbriae whose terminal sub-unit FimH adhesin that binds specifically to mannose also contributes to the adhesion onto abiotic surfaces through nonspecific interactions.[62] For the sake of clarity, we stress that the only force curves with one or several adhesive events (*i.e.* those carried out for Δ_4*adh*_PcL*yad* cells) were subjected to modelling on the basis of eq 1, and the other force curves are therefore not considered in the following modelling developments and related discussion.

The force curves carried out on Δ_4*adh*_PcL*yad* cells are generally defined by a saw tooth pattern with one or several peaks that reflect the adhesive events, irrespective of the nature of the considered AFM-probe (**Figure 3)**. These peaks translate the molecular elongation of the Yad fimbriae upon withdrawal of the AFM-probe and the subsequent rupture of the fimbriae-probe as marked by an abrupt decrease of the measured force. The presence of successive adhesive events (and related force maxima) is simply connected to the possible anchoring of the molecules-functionalized AFM probe with several Yad fimbriae defined by various lengths, as previously discussed (**Figures 1** and **S1)** and by successive adhesive/rupture events due to the unspooling along the backbone of a single fimbria. **Figure 3** evidences that the elongation of Yad fimbriae structures takes place up to *ca.* 1200-3000 nm distance depending on the chemistry of the AFM probe, which excludes any contribution of the AFM-probe linkers (with

View Article Online
DOI: 10.1039/D0NR06840C

length of 6.3 nm in fully extended configuration) to detected adhesion/rupture events. The connection between the occurrence of adhesive events revealed by SMFS and the presence of Yad fimbriae for Δ_4*adh*_PcL*yad* cells is supported by the negative control SMFS measurements performed on Δ_4*adh* bacteria that do not express Yad fimbriae nor any other external structures at their surface: force curves measured for Δ_4*adh* cells are indeed systematically flat, regardless of the tested functionalities of the AFM probe (**Figure S5**).

The analysis of the whole set of force curves collected by SMFS (this set represents *ca.* 5000 to 8000 forces curves depending on the tested condition, see details in **Table 2**), makes it possible the determination of the statistic distribution of the number of detected adhesive events as a function of the molecular functionality of the AFM-probe (**Figure S6),** as well as that pertaining to the magnitude of the measured adhesion forces (**Figure 4)** whose averaged values are given in **Table 2** for the various interaction configurations tested. For the AFM-probe functionalized with polyclonal antibodies (anti-YadC and anti-YadN), a monomodal distribution of the number of adhesive events was observed with an average of about 3-4 adhesive events per force curve (**Figure S6**). However, the distribution of the magnitude of the corresponding adhesion forces does not display a single maximum but, instead, is multimodal (**Figure 4**). Most (~ 65%) of the adhesive events correspond to 75-200 pN adhesion force amplitude while others are associated to forces in the 200-400 pN range (**Figure 4**). Concerning SMFS results pertaining to AFM-probe functionalized with xylosyl, a bimodal distribution of the number of adhesive events is clearly observed, with a first population of about 3-4 adhesive events per force curve and a second one with *ca.* 8-12 adhesive events in average (**Figure S6**). We find that most (~ 65%) of these adhesive events correspond to the two modes of the distribution of adhesion forces, at about 75 pN and 160 pN, while the others are distributed over the 200-400 pN force range (**Figure 4**). The range of adhesion force achieved with the Yad

View Article Online
DOI: 10.1039/D0NR06840C

fimbriae-anti-YadC,N and Xylose pairs is strikingly comparable to that reported for type 1 fimbriae-mannosylated surface (adhesion force up to 400 pN).[45]

The SMFS measurements performed with the AFM-probes functionalized with mannosyl, galactosyl and lactosyl residues reveal similar patterns with a monomodal distribution of about 3-4 adhesive events per force curve (**Figure S6**). In addition, about 80% of these adhesive events are defined by adhesion forces of 50-75 pN and the other events are distributed over force amplitudes covering the 75 to 200 pN range (**Figure 4**). Altogether, the analysis evidences that the interactions between Yad fimbriae and polyclonal antibodies (anti-YadC and anti-YadN) or xylosyl residue grafted at the apex of the AFM-probes are stronger and much more frequent than those taking place between Yad and the other glycosyl residues selected in this work (**Table 2**). In addition, there is no significant difference between the adhesion force measured between Yad fimbriae and anti-YadC, anti-YadN or Xyl-covered surfaces. This finding supports the specific nature of the Yad fimbriae-antibodies and Yad fimbriae-Xyl interactions, which is consistent with the conclusions derived on the basis of cell adhesion properties addressed at the macroscopic scale (**Figure 2**).

Assessment of Yad fimbriae nanomechanical features from Worm-Like-Chain modeling.

The SMFS force curves reported in **Figure 3** were interpreted on the basis of the Worm like Chain (WLC) model (eq 1). The theoretical reconstruction of the saw tooth like dependence of the force on separation distance leads to the evaluation of the statistical distribution of three key parameters pertaining to the structural properties of Yad fimbriae, namely: their contour length L_c or, equivalently, their maximal extension/stretching upon withdrawal of the functionalized AFM-probe (**Figure 5**), their molecular periodicity (or peak-to-peak distance) that refers to the distance separating two successive adhesive events taking place along a single fimbria backbone or between the AFM probe and molecules belonging to different Yad fimbriae

(**Figure 6**), and their persistence length which basically refers to the dimension of the shortest Yad fimbriae units behaving as rigid rod (**Figure S7**). Comparison between the obtained persistence length and size of the YadN subunit (**Table 4**) qualitatively reflects the flexibility of these polymeric subunits of the Yad fimbriae under stretching conditions. For completeness, **Table 2** collects the average values of the maxima of the aforementioned distributions in contour length, persistence length and peak-to-peak separation distance.

The SMFS measurements performed with AFM probes defined by antibodies (anti-YadC and anti-YadN) functionalities grafted at their apex allow the specific targeting and pulling on YadC and YadN sub-units of the Yad fimbriae (**Figure 7**). The contour length retrieved from analysis of the corresponding force curves is distributed over a wide range spanning from a few nanometers to 2000 nm (**Figure 5**), which obviously renders difficult a clear Gaussian-based assignment of the various modes that define the distribution. Distributions fitting to multimodal Gaussian components should therefore be considered at a qualitative level. Despite of this difficulty, inherent to the SMFS analysis of molecular structures polydisperse in size, two distributions of the contour length of Yad fimbriae stretched by anti-YadN-decorated AFM-probe can be defined: one centered at 247 nm and the other at 761 nm. With using anti-YadC AFM probe, the distributions are clearly shifted to higher values of the contour length, with the possible assignment of three main modes at 936, 1234 and 1648 nm. Assuming that anti-YadC AFM-probe unspools the subunits constituting the fimbriae from the very top end of the Yad structure (**Figure 7**), the three distributions observed for the contour length suggest the presence of Yad fimbriae whose most frequently encountered dimensions correspond to the maxima of the detected distributions. If complete unspooling of the backbone of the fimbriae takes place, it implies that the probed Yad fimbriae are composed of *ca.* 120, 158 and 210 YadN sub-units. Analysis of the force measurements performed with anti-YadN AFM-probe leads to shorter fimbriae contour lengths. This finding is fully consistent with an unspooling of the probed

View Article Online
DOI: 10.1039/D0NR06840C

fimbriae that does not start from their very top end but, instead, from an intermediate position along their main body (**Figure 7**).

Three main values are further found for the persistence length of Yad fimbriae unspooled by anti-Yad(C and N) AFM probe (**Figure S7**): 0.4, 0.6 and 1.0 nm. These values are significantly higher (by *ca.* 1 order of magnitude) than those previously reported for bacterial type 1 or type IV fimbriae[60, 63, 64] and, most importantly, they define persistence lengths that are significantly shorter than a single pilin subunit (7.8 nm, as reported in **Table 4**). Recent AFM and simulation studies demonstrated that a 1 nm value corresponds to a single strand within a fimbria and that lower values of persistence length may be associated to intramolecular deformations and unfolding of pilin subunits.[45, 65-67] As further reported in previous studies based on AFM measurements, low persistence length values may originate from the stretching of polypeptide segments (as a result of the applied force) and not from the stretching of a polymer chain consisted of globular units.[68] Accordingly, our results indicate that Yad fimbriae consist of a tubular assembly of easily deformable subunits (*i.e.* with persistence length that is significantly shorter than the subunit size), which fragilize the whole Yad structure when subjected to mechanical stress. This is in line with our observation of broken Yad fimbriae at the substrates surface and of a resulting marked polydispersity in terms of Yad fimbriae length (**Figure 1**).

Previous observations of Yad fimbriae using Transmission Electron Microscopy (TEM) suggested that Yad fimbriae could be much more flexible than, for example, type 1 fimbriae.[30, 41] Even though conclusions derived from TEM or cryo-TEM analysis should be considered with caution due to the sample preparation procedures that possibly modify biosurface structure and integrity, this finding is consistent with the absence of successive force plateau regimes in the SMFS force profiles pertaining to Yad, as invoked above. The shorter persistence length of type 1 fimbriae conjugated with the observation of SMFS force plateau regimes for such a structure indicate a larger molecular cohesion and tensile strength as compared to those for Yad

structure whose easier unfolding of the composing YadN subunits makes it impossible for the overall Yad structure to maintain cohesion upon withdrawal of the AFM probe, which explains, in turn, the absence of any force plateau in the SMFS profile and the detection of successive abrupt rupture events.

The periodicity of the adhesive events along fimbriae backbone, denoted as δL, was evaluated from the distance between two successive adhesive events (**Figure 6** and **Table 2**). For situations where Yad fimbriae are unspooled by anti-YadC and anti-YadN AFM-probes, the large distribution in δL (from few manometers to 1 μm) is multimodal with four maxima at *ca.* 30, 120, 350 and 700 nm. It is found that 40-50% of the probed δL values are in the 0-100 nm range, which indicates that fimbriae unspooling occurs mainly by successive 'jumps' of ensembles of 12 YadN subunits. In cases where fimbriae are unspooled by xylosyl AFM-probe, the distribution in δL remains trimodal but, here, the three detected modes are much more clearly defined (77, 243 and 331 nm) with δL values that cover a narrower range (from few nanometers to 500 nm) that that obtained with anti-Yad probes. The well-defined trimodal distribution suggests that unspooling of the Yad fimbriae by Xyl probes takes place upon by successive jump of 10, 31 and 42 YadN subunits. The lesser defined δL distributions measured with the anti YadN and anti YadC probes may originate from the polyclonal nature of the used antibodies that may interact simultaneously with several YadN and YadC subunits, in contrast with xylose that targets only one YadC subunit.

Modelling of the SMFS force curves collected with the other galactosyl (Gal, Man and Lac)-grafted AFM-probes shows that the corresponding multimodal distribution of δL (**Figure 6**), with rather ill-defined Gaussian components, basically spread over a large range of values (from few nanometers to 1 μm) with maxima located at larger δL as compared to those identified for Xyl and anti-Yad probes. The dispersion in δL values is somewhat lesser pronounced for mannosyl- and lactosyl-grafted AFM-probes (few nanometers up to 600 nm) than for galactosyl

View Article Online
DOI: 10.1039/D0NR06840C

AFM probe. Three maxima of about 200, 350 and 600 nm are found for δL derived from SMFS force curves measured with galactosyl-grafted AFM-probe, and values of about 130, 230 and 400 nm are obtained with the mannosyl-grafted AFM-probe. The interpretation of SMFS experiments performed with the glycosylated AFM-probes is rather complicated, except for the probe grafted with xylosyl specifically recognized by YadC subunit. Instead, galactosyl, lactosyl and mannosyl residues may interact with any of the Yad fimbriae subunits (which includes the YadM, YadK, YadL and YadN components), resulting in unspooling configuration close to that depicted for anti-YadN grafted AFM probe (**Figure 7**). Accordingly, unspooling of the Yad fimbriae by galactosyl-, mannosyl- and lactosyl-grafted AFM-probes possibly occur by successive jumps of sets of 17 up to 104 YadN subunits. It should be further realized that the interpretation of the force curves measured with these functionalities of the AFM probe is all the more difficult as the interactions between glycosylated AFM-probes and Δ_4*adh*_PcL*yad* bacterial cell wall may involve macromolecular structures expressed at the cell wall other than the targeted Yad fimbriae. This hypothesis is comforted by the inspection of the adhesion results obtained with Δ_4*adh*, which features rare adhesive events (but still measurable) between Δ_4*adh* cell wall and the various substrates adopted in this work (see **Table 3**). Complementary experiments using various cell surface components on mutant strains and surfaces with controlled chemistries other than those tested here could be more relevant to address this issue. We emphasize still the probability of interactions occurrence between galactosyl-, mannosyl- and lactosyl-grafted AFM-probes concerns less than 20% of total force curves, which is 4 to 5 times lower than that relevant for the curves obtained with anti-YadN, anti-YadC and xylosyl residue. Here, accordingly, we clearly evidenced that Yad fimbriae interact primarily and strongly with anti-YadN, anti-YadC and xylosylated surfaces whereas interactions in respect with other glycosylated surfaces are significantly lesser frequent and are defined by lower magnitude of the corresponding adhesion forces.

View Article Online
DOI: 10.1039/D0NR06840C

On the connection between adhesion properties of Yad fimbriae and Δ_4*adh*_PcL*yad* cells revealed at the molecular and macroscopic scales, respectively.

Figure 8 reports the concentrations of Δ_4*adh*_PcL*yad* bacteria adhered at the surface of SAM-Xyl, SAM-anti YadC and SAM-anti YadN (**Figure 2**) as a function of the median adhesion forces measured by SMFS at the molecular scale between Yad fimbriae and Xyl-, anti YadC- and anti YadN-AFM probes, respectively (**Figure 4**). The data obtained for the other glycosylated surfaces and glycosyl-decorated AFM probes further complete the comparison between Yad fimbriae adhesion features assessed at the molecular scale and the macroscopic Δ_4*adh*_PcL*yad* cells adhesion properties evaluated from standard fluorescence-based counting method. The dispersion of the points in the *x*-axis of **Figure 8** reflects the range of maximal adhesion forces measured over the various multimodal distribution's maxima pictured in **Figure 4**.

Figure 8 evidences the existence of an exponential-like dependence for the surface concentration of adhered cells on the corresponding adhesion force measured at the relevant molecular scale. For the sake of quantitative illustration, 100 pN interaction force between a single bacterium cell wall (as selected for the SMFS experiments) and substrate surface leads to the adhesion of about 10^6 cells cm^{-2}, and 200 pN leads to the adhesion of about 10^8 cells cm^{-2}. The latter surface concentration corresponds to a fully covered surface if assuming that all adhered bacteria adopt a lying cylindrical configuration at the substrate surface. To the best of our knowledge, the influence of substrate surface chemistry on bacterial adhesion has been rarely addressed both at the macroscopic and molecular scales[69, 70] and the experimental results detailed in this work highlight the intimate connection between the nanoscale adhesion features of the Yad fimbriae and the resulting bacterial adhesion behavior. They therefore support numerous theoretical studies about the dependence of bacterial adhesion on surface chemistry[71-

View Article Online
DOI: 10.1039/D0NR06840C

[74] left, so far, without solid experiments-based evidence of the relationship between adhesion properties detailed at the various scales of interest, from the molecular adhesion event to the cell adsorption process. The exponential relationship revealed by **Figure 8** further suggests the applicability of an effective Boltzmann-like dependence for the surface concentration of adhered bacteria on the operational molecular adhesion force F_{adh}, recalling that F_{adh} may be formally converted into an adhesion energy per unit surface area upon dividing F_{adh} by a characteristic length scale, this ratio having the dimension of a superficial tension. Last, the results obtained in this work support that assessment of bacterial adhesion features can not be reduced to the standard DLVO-inspired strategy that consists in measuring surface charge of the bacteria (with all ''ins and outs'' related to this issue, see e.g. the demonstration by Duval and coworkers that the zeta-potential concept is physically irrelevant for bacteria,[56] and references therein[59] and surface charge of the deposition substrate. Previous work on aggregation of bacteria decorated or not by self-associating Ag43 adhesins demonstrated that reasoning on the basis of the (similar) pH-dependent macroscopic surface charge of bacteria (evaluated by electrophoresis) decorated or not by Ag43 could not explain the differentiated auto-aggregation properties of these cells.[75] Instead a detailed SFMS-based analysis could clarify the molecular origin of the observed aggregation features of bacteria devoid or not of Ag43. In addition, the salinity conditions operational in our SMFS measurements (with overall ionic strength well above 100 mM) are such that the surface charge of the bacteria are significantly screened, meaning that short range coulombic forces, dipole-dipole interactions and, obviously, specific interaction forces are here the relevant determinants of Yad fimbriae binding to the selected substrates. In line with these results, our results clearly evidence a strong connection between the adhesion forces measured at the molecular scale (not accounted for in standard DLVO theory) and the macroscopic adhesion properties of Yad-decorated bacteria.

View Article Online
DOI: 10.1039/D0NR06840C

Conclusion

The adhesion of Yad fimbriae on model substrates defined by different and controlled surface chemistries are here evaluated at the molecular scale by Single Molecule Force Spectroscopy. The results evidence that the affinity of Yad fimbriae for xylose is as strong as that for polyclonal anti-YadC and anti-YadN antibodies (*ca.* 80 to 300 pN). In contrast, the adhesion features of Yad fimbriae on -NH_2, -OH, -COOH, -CH_3, Lactose, Mannose and Galactose terminated self-assembled monolayers indicate non specificity of the interactions of Yad with these surfaces. A clear connection between these findings, relevant at the molecular scale, and the adhesion properties of *E. coli* decorated or not by Yad fimbriae is further established. This nano-macro relationship pinpoints the importance of the study of nanoscale specific interactions of fimbriae with their cognate ligands. Such a study opens the way to the design of efficient anti-adhesive molecules that could be used in anti-virulence strategies against pathogenic bacteria.

Acknowledgments

The authors thank the Spectroscopy and Microscopy Service Facility (SMI) of LCPME (Université de Lorraine-CNRS – http://www.lcpme.cnrs-nancy.fr) where most of experiments were performed. GF and JFLD further thank C. Caillet of the LIEC for preliminary assessment of the fragility of parietal structures decorating Δ_4*adh* and Δ_4*adh*_PcL*yad* cells. We thank F. Larsonneur for Δ_4*adh*_PcL*yad* strain construction. Work in the group of CB was supported by an Institut Pasteur grant, by the French government's Investissement d'Avenir Program, Laboratoire d'Excellence "Integrative Biology of Emerging Infectious Diseases" (grant n°ANR-10-LABX-62-IBEID) and the *Fondation pour la Recherche Médicale* (grant no. DEQ20180339185). YC was supported by a MENESR (Ministère Français de l'Education Nationale, de l'Enseignement Supérieur et de la Recherche) fellowship.

View Article Online
DOI: 10.1039/D0NR06840C

Supporting Information

Supplementary AFM images of Δ_4*adh* and Δ_4*adh*_PcL*yad* cells (**Figure S1**), IRRAS spectra of the various model SAM substrates selected in this study (**Figure S2**), Representative epifluorescence images of Δ_4*adh*_PcL*yad* on the different SAM substrates tested (**Figure S3**), Representative epifluorescence images of Δ_4*adh* on the different SAM substrates tested (**Figure S4**), Illustrative SMFS force measurements for Δ_4*adh* cell wall interacting with AFM probes featuring YadC, YadN, xylose, galactose, mannose and lactose functionalities (**Figure S5**), Statistic distribution of the number of adhesive events per retraction force curve recorded for Δ_4*adh*_PcL*yad* cell wall in interaction with AFM probes featuring YadC, YadN, xylose, galactose, mannose and lactose functionalities (**Figure S6**), As in **Figure S6**, *albeit* for the persistence length of Yad fimbriae (**Figure S7**).

View Article Online
DOI: 10.1039/D0NR06840C

References:

1. D. M. Costa, K. Johani, D. S. Melo, L. K. O. Lopes, L. K. O. Lopes Lima, A. F. V. Tipple, H. Hu and K. Vickery, *Lett. Appl. Microbiol.*, 2019, **68**, 269-276.

2. S. Galié, C. García-Gutiérrez, E. M. Miguélez, C. J. Villar and F. Lombó, *Frontiers in microbiology*, 2018, **9**, 898-898.

3. D. Lebeaux, J.-M. Ghigo and C. Beloin, *Microbiol. Mol. Biol. Rev.*, 2014, **78**, 510-543.

4. J. Luis Del Pozo, *Expert Review of Anti-Infective Therapy*, 2018, **16**, 51-65.

5. A. Alvarez-Ordonez, L. M. Coughlan, R. Briandet and P. D. Cotter, in *Annual Review of Food Science and Technology, Vol 10*, eds. M. P. Doyle and D. J. McClements, 2019, vol. 10, pp. 173-195.

6. J. W. Leff and N. Fierer, *PLoS One*, 2013, **8**, e59310.

7. J. J. Luna-Guevara, M. M. P. Arenas-Hernandez, C. Martínez de la Peña, J. L. Silva and M. L. Luna-Guevara, *International Journal of Microbiology*, 2019, **2019**, 2894328.

8. C. Berger, S. Sodha, R. Shaw, P. Griffin, D. Pink, P. Hand and G. Frankel, *Environmental microbiology*, 2010, **12**, 2385-2397.

9. G. Ávila-Quezada, E. Sánchez, A. A. Gardea-Béjar and E. Acedo-Félix, *New Zealand Journal of Crop and Horticultural Science*, 2010, **38**, 47-55.

10. S. Kampmeier, M. Berger, A. Mellmann, H. Karch and P. Berger, *Curr Top Microbiol Immunol*, 2018, **416**, 117-148.

11. J. P. Cramer, in *Emerging Infectious Diseases*, eds. Ö. Ergönül, F. Can, L. Madoff and M. Akova, Academic Press, Amsterdam, 2014, DOI: https://doi.org/10.1016/B978-0-12-416975-3.00017-0, pp. 213-227.

12. E. Köckerling, L. Karrasch, A. Schweitzer, O. Razum and G. Krause, *Frontiers in Public Health*, 2017, **5**.

13. A. Caprioli, G. Scavia and S. Morabito, *Microbiology spectrum*, 2014, **2**.

14. J. B. Kaper and A. D. O'Brien, *Microbiology spectrum*, 2014, **2**.

15. E. J. Boll, J. Ayala-Lujan, R. L. Szabady, C. Louissaint, R. Z. Smith, K. A. Krogfelt, J. P. Nataro, F. Ruiz-Perez and B. A. McCormick, *mBio*, 2017, **8**, e00717-00717.

16. M. A. Rendon, Z. Saldana, A. L. Erdem, V. Monteiro-Neto, A. Vazquez, J. B. Kaper, J. L. Puente and J. A. Giron, *Proc. Natl. Acad. Sci. USA*, 2007, **104**, 10637-10642.

17. C. Lang, A. Fruth, G. Holland, M. Laue, S. Mühlen, P. Dersch and A. Flieger, *Emerging Microbes & Infections*, 2018, **7**, 1-16.

18. S. Knutton, R. Shaw, M. K. Bhan and A. S. McNeish, *Pediatr. Res.*, 1990, **27**, 530-530.

19. C. Moreira, S. Carneiro, J. Nataro, L. Trabulsi and W. Elias, *FEMS Microbiol. Lett.*, 2003, **226**, 79-85.

20. P. Luthje and A. Brauner, in *Advances in Microbial Physiology, Vol 65: Advances in Bacterial Pathogen Biology*, ed. R. K. Poole, 2014, vol. 65, pp. 337-372.

21. P. Klemm, V. Hancock and M. A. Schembri, *Environ. Microbiol. Rep.*, 2010, **2**, 628-640.

22. V. Ageorges, R. Monteiro, S. Leroy, C. M. Burgess, M. Pizza, F. Chaucheyras-durand and M. Desvaux, *FEMS Microbiol. Rev.*, 2020, **44**, 314-350.

23. A. Monserrat-Martinez, Y. Gambin and E. Sierecki, *Int. J. Mol. Sci.*, 2019, **20**, 1255.

24. J. J. Psonis and D. G. Thanassi, *EcoSal Plus*, 2019, **8**.

25. S. Geibel and G. Waksman, *Biochim. Biophys. Acta-Mol. Cell Res.*, 2014, **1843**, 1559-1567.

26. C. G. Korea, J. M. Ghigo and C. Beloin, *BioEssays*, 2011, **33**, 300-311.

27. D. J. Wurpel, S. A. Beatson, M. Totsika, N. K. Petty and M. A. Schembri, *PLoS One*, 2013, **8**.

28. F. Dziva, H. Hauser, T. R. Connor, P. M. van Diemen, G. Prescott, G. C. Langridge, S. Eckert, R. R. Chaudhuri, C. Ewers, M. Mellata, S. Mukhopadhyay, R. Curtiss, III, G. Dougan, L. H. Wieler, N. R. Thomson, D. J. Pickard and M. P. Stevens, *Infect. Immun.*, 2013, **81**, 838-849.

29. R. Verma, T. C. Galvao Rojas, R. P. Maluta, J. L. Leite, L. P. Mendes da Silva, G. Nakazato and W. D. da Silveira, *Infect. Immun.*, 2016, **84**, 187-193.

30. F. Larsonneur, F. Martín, A. Mallet, M. Martinez-gil, V. Semetey, J. M. Ghigo and C. Beloin, *Environmental Microbiology*, 2016, **18**, 5228-5248.

31. K. C. Gross and C. E. Sams, *Phytochemistry*, 1984, **23**, 2457-2461.

32. A. P. S. Sandhu, G. S. Randhawa and K. S. Dhugga, *Molecular Plant*, 2009, **2**, 840-850.

33. E. M. S. M. Gaspar, I. S. Nunes and J. F. Lopes, *Xylose: Production, Consumption and Health Benefits*, 2012, 43-67.

34. C. F. Carson and T. V. Riley, *Communicable diseases intelligence quarterly report*, 2003, **27 Suppl**, S143-146.

35. I. Ofek, D. L. Hasty and N. Sharon, *FEMS Immunol. Med. Microbiol.*, 2003, **38**, 181-191.

36. A. Asadi, S. Razavi, M. Talebi and M. Gholami, *Infection*, 2019, **47**, 13-23.

37. C. K. Cusumano, J. S. Pinkner, Z. Han, S. E. Greene, B. A. Ford, J. R. Crowley, J. P. Henderson, J. W. Janetka and S. J. Hultgren, *Science Translational Medicine*, 2011, **3**, 109ra115-109ra115.

38. J. Ohlsson, J. Jass, B. E. Uhlin, J. Kihlberg and U. J. Nilsson, *ChemBioChem*, 2002, **3**, 772-779.

39. M.-C. Duvernoy, T. Mora, M. Ardre, V. Croquette, D. Bensimon, C. Quilliet, J.-M. Ghigo, M. Balland, C. Beloin, S. Lecuyer and N. Desprat, *Nature Communications*, 2018, **9**, 1-10.

40. P. P. Cherepanov and W. Wackernagel, *Gene*, 1995, **158**, 9-14.

41. C. G. Korea, R. Badouraly, M. C. Prevost, J. M. Ghigo and C. Beloin, *Environ Microbiol*, 2010, **12**, 1957-1977.

42. L. Wildling, B. Unterauer, R. Zhu, A. Rupprecht, T. Haselgrubler, C. Rankl, A. Ebner, D. Vater, P. Pollheimer, E. E. Pohl, P. Hinterdorfer and H. J. Gruber, *Bioconjug Chem*, 2011, **22**, 1239-1248.

43. A. Ebner, L. Wildling, R. Zhu, C. Rankl, T. Haselgrubler, P. Hinterdorfer and H. J. Gruber, in *Stm and Afm Studies On*, Springer-Verlag Berlin, Berlin, 2008, vol. 285, pp. 29-76.

44. A. Ebner, L. Wildling, A. S. Kamruzzahan, C. Rankl, J. Wruss, C. D. Hahn, M. Holzl, R. Zhu, F. Kienberger, D. Blaas, P. Hinterdorfer and H. J. Gruber, *Bioconjug Chem*, 2007, **18**, 1176-1184.

45. A. Jacquot, C. Sakamoto, A. Razafitianamaharavo, C. Caillet, J. Merlin, A. Fahs, J. M. Ghigo, C. Beloin, J. F. L. Duval and G. Francius, *J. Biomed. Nanotechnol.*, 2014, **10**, 3361-3372.

46. A. Ebner, P. Hinterdorfer and H. J. Gruber, *Ultramicroscopy*, 2007, **107**, 922-927.

47. H. Schillers, I. Medalsy, S. Hu, A. L. Slade and J. E. Shaw, *J. Mol. Recognit.*, 2016, **29**, 95-101.

48. K. Xu, W. Sun, Y. Shao, F. Wei, X. Zhang, W. Wang and P. Li, *Nanotechnology Reviews*, 2018, **7**, 605-621.

49. P. Polyakov, C. Soussen, J. Duan, J. F. L. Duval, D. Brie and G. Francius, *PLoS One*, 2011, **6**, e18887.

50. A. Janshoff, M. Neitzert, Y. Oberdorfer and H. Fuchs, *Angew Chem Int Ed Engl*, 2000, **39**, 3212-3237.

51. C. Ortiz and G. Hadziioannou, *Macromolecules*, 1999, **32**, 780-787.

52. E. Wiercigroch, E. Szafraniec, K. Czamara, M. Z. Pacia, K. Majzner, K. Kochan, A. Kaczor, M. Baranska and K. Malek, *Spectrochimica acta. Part A, Molecular and biomolecular spectroscopy*, 2017, **185**, 317-335.

View Article Online
DOI: 10.1039/D0NR06840C

759 53. H. A. Wells and R. H. Atalla, *J. Mol. Struct.*, 1990, **224**, 385-424.

760 54. R. Zimmermann, J. F. L. Duval and C. Werner, *Curr. Opin. Colloid Interface Sci.*, 2019,
761 **44**, 177-187.

762 55. J. Song, J. F. L. Duval, M. A. Stuart, H. Hillborg, U. Gunst, H. F. Arlinghaus and G. J.
763 Vancso, *Langmuir*, 2007, **23**, 5430-5438.

764 56. J. F. L. Duval and F. Gaboriaud, *Curr. Opin. Colloid Interface Sci.*, 2010, **15**, 184-195.

765 57. F. Gaboriaud, M. L. Gee, R. Strugnell and J. F. L. Duval, *Langmuir*, 2008, **24**, 10988-
766 10995.

767 58. M. Castelain, S. Ehlers, J. Klinth, S. Lindberg, M. Andersson, B. E. Uhlin and O. Axner,
768 *European biophysics journal : EBJ*, 2011, **40**, 305-316.

769 59. F.-J. Chen, C.-H. Chan, Y.-J. Huang, K.-L. Liu, H.-L. Peng, H.-Y. Chang, G.-G. Liou,
770 T.-R. Yew, C.-H. Liu, K. Hsu and L. Hsu, *J. Bacteriol.*, 2011, **193**, 1718-1725.

771 60. M. Andersson, O. Björnham, M. Svantesson, A. Badahdah, B. E. Uhlin and E. Bullitt,
772 *J. Mol. Biol.*, 2012, **415**, 918-928.

773 61. M. Forero, O. Yakovenko, E. V. Sokurenko, W. E. Thomas and V. Vogel, *PLoS Biol.*,
774 2006, **4**, e298.

775 62. L. A. Pratt and R. Kolter, *Mol. Microbiol.*, 1998, **30**, 285-293.

776 63. P. M. Silverman and M. B. Clarke, *Integrative Biology*, 2010, **2**, 25-31.

777 64. Hendrick W. de Haan, *Biophys. J.*, 2016, **111**, 2263-2273.

778 65. J. Rheinlaender, A. Gräbner, L. Ott, A. Burkovski and T. E. Schäffer, *European*
779 *biophysics journal : EBJ*, 2012, **41**, 561-570.

780 66. M. Castelain, M.-P. Duviau, A. Canette, P. Schmitz, P. Loubière, M. Cocaign-Bousquet,
781 J.-C. Piard and M. Mercier-Bonin, *PLoS One*, 2016, **11**, e0152053-e0152053.

782 67. W. Pönisch, C. A. Weber, G. Juckeland, N. Biais and V. Zaburdaev, *New Journal of*
783 *Physics*, 2017, **19**, 015003.

784 68. , !!! INVALID CITATION !!! 57, 59, 60.

785 69. F. Alam, S. Kumar and K. M. Varadarajan, *ACS Biomater. Sci. Eng.*, 2019, **5**, 2093-
786 2110.

787 70. R. Bos, H. C. van der Mei and H. J. Busscher, *FEMS Microbiol. Rev.*, 1999, **23**, 179-
788 230.

789 71. F. Pan, S. Altenried, M. Liu, D. Hegemann, E. Bülbül, J. Moeller, W. W. Schmahl, K.
790 Maniura-Weber and Q. Ren, *Materials Horizons*, 2020, **7**, 93-103.

72. J. K. Oh, Y. Yegin, F. Yang, M. Zhang, J. Li, S. Huang, S. V. Verkhoturov, E. A. Schweikert, K. Perez-Lewis, E. A. Scholar, T. M. Taylor, A. Castillo, L. Cisneros-Zevallos, Y. Min and M. Akbulut, *Sci Rep*, 2018, **8**, 17247.

73. A. O. Eskhan and N. I. Abu-Lail, *Colloid Polym. Sci.*, 2014, **292**, 343-353.

74. H. J. Busscher, W. Norde and H. C. van der Mei, *Appl. Environ. Microbiol.*, 2008, **74**, 2559-2564.

75. A. Jacquot, C. Sakamoto, A. Razafitianamarahavo, C. Caillet, J. Merlin, A. Fahs, J. M. Ghigo, J. F. L. Duval, C. Beloin and G. Francius, *Nanoscale*, 2014, **6**, 12665-12681.

76. G. Yachdav, E. Kloppmann, L. Kajan, M. Hecht, T. Goldberg, T. Hamp, P. Hönigschmid, A. Schafferhans, M. Roos, M. Bernhofer, L. Richter, H. Ashkenazy, M. Punta, A. Schlessinger, Y. Bromberg, R. Schneider, G. Vriend, C. Sander, N. Ben-Tal and B. Rost, *Nucleic Acids Res.*, 2014, **42**, W337-W343.

View Article Online
DOI: 10.1039/D0NR06840C

Tables

Table 1. Details on the genetic profiles of Δ_4*adh* and Δ_4*adh*_PcL*yad* strains and on their constructions.

Strain or plasmid	Relevant genotypic and phenotypic characteristics	Source or reference
Δ_4*adh*	MG1655_*gfp*_Δ*fliE-R*::*cat*_Δ*flu*::FRT_Δ*fimAICDFGH*::*zeo*_Δ*csgA*::*aadA7* GFP+, no flagella, no type 1 fimbriae, no Ag43, no curli, Amp^R, Cm^R, Zeo^R, $Spec^R$	39
PcL*yad*	MG1655_*km*PcL*yad*, *yad* operon under the control of the constitutive lambda P_R promoter, Km^R	41
Δ_4*adh*_PcL*yad*	MG1655_*gfp*_Δ*fliE-R*::*cat*_Δ*flu*::FRT_Δ*fimAICDFGH*::*zeo*_Δ*csgA*::*aadA7*_*km*PcL*yad*, Km^R P1vir transduction of *km*PcL*yad* from strain PcL*yad* into $\underline{\Delta_4 adh}$ GFP+, no flagella, no type 1 fimbriae, no Ag43, no curli, constitutive expression of the *yad* operon, Amp^R, Cm^R, Zeo^R, $Spec^R$, Km^R	This work

Table 2. Physico-chemical parameters derived from Single Molecule Force Spectroscopy (SMFS) measurements performed on Δ_4*adh*_PcL*yad* bacteria using different functionalities of the AFM probe (indicated). **The evaluation of the parameters is performed by modeling the measured force-curves using eq 1, and given values correspond to maxima of the corresponding multimodal distributions and their standard deviations. * The values reported in this column refer to the % of the force curves featuring at least one adhesive event. See text for further details.

AFM-Probes (# curves)	Adhesive events (%)*	Adhesion forces (nN)**	Maximal extension (nm)**	Persistence length (nm)**	Peak-to-peak distance (nm)
Anti-YadC (6487)	98.0 ± 1.1	0.081 ± 0.061 0.148 ± 0.079 0.245 ± 0.084	936 ± 170 1234 ± 205 1648 ± 77	0.45 ± 0.12 0.60 ± 0.29 1.05 ± 0.78	37 ± 40 118 ± 112 366 ± 178 709 ± 255
Anti-YadN (8210)	92.5 ± 3.5	0.078 ± 0.045 0.157 ± 0.078 0.302 ± 0.081	247 ± 102 761 ± 233	0.38 ± 0.20 0.67 ± 0.32 1.31 ± 1.07	23 ± 54 122 ± 107 344 ± 171 690 ± 261
Xyl (6715)	87.3 ± 5.7	0.097 ± 0.066 0.180 ± 0.072 0.339 ± 0.121	371 ± 66 605 ± 85 827 ± 72 1006 ± 68 1194 ± 59	0.35 ± 0.23 1.11 ± 0.85	77 ± 49 243 ± 53 331 ± 48
Gal (4772)	19.1 ± 4.2	0.058 ± 0.054 0.177 ± 0.104	673 ± 162 945 ± 154 1287 ± 238	0.29 ± 0.16 0.62 ± 0.35 0.98 ± 0.65	191 ± 90 355 ± 185 613 ± 192
Lac (6062)	22.7 ± 6.8	0.064 ± 0.072 0.159 ± 0.091	589 ± 106 792 ± 98 953 ± 89 1178 ± 182 1407 ± 208	0.38 ± 0.17 0.64 ± 0.29	131 ± 104 235 ± 83 403 ± 222

Man (5258)	15.3 ± 3.9	0.076 ± 0.081 0.183 ± 0.078	241 ± 132 435 ± 106 576 ± 97	0.35 ± 0.11 0.58 ± 0.25 0.95 ± 0.67	216 ± 94 285 ± 83 411 ± 184 815 ± 71

Table 3. As in Table 2 *albeit* for Δ_4*adh* cells. 'nd': 'not determined.

AFM-Probes (# curves)	**Adhesive events (%)***	**Adhesion forces (nN)****	**Maximal extension (nm)****	**Persistence length (nm)****	**Peak-to-peak distance (nm)**
Anti-YadC (2772)	0.7 ± 0.9	nd	nd	nd	nd
Anti-YadN (3894)	2.1 ± 1.7	nd	nd	nd	nd
Xyl (2721)	1.3 ± 1.5	nd	nd	nd	nd
Gal (2772)	4.9 ± 2.2	nd	nd	nd	nd
Lac (3267)	2.7 ± 0.8	nd	nd	nd	nd
Man (3662)	5.0 ± 3.3	nd	nd	nd	nd

824 **Table 4.** Amino acids sequences, characteristics and most probable structures of YadC and YadN sub-unit of Yad fimbriae determined using

825 PredictProtein, an online open resource for prediction of protein structural and functional features according to integrated methods.[76]

Peptide	Amino acid sequence	Structure	Characteristics
YadC	MKTIFRYILF LALYSCCNTV SAYTSFIVGN NAGVDNYRGP STAAQMTFNY TSTASNLVFY KPTQLGPTGV KMYWSYLDTG TGGGILYCNT SGRANPGPIT IENAMVYSGK DYGGHKLFNT SVPGLYYTML ISRVWSAYDT ITDIQSPGIY IGDPSNQEFF FSVTDSDLQT KGCNKADDYD KFWAIGGIVH NITVEFYTDT NFDPTLNQQV QLSSSSNYLY SFKAYSPGTK VVDHSNHIYV NFTLNNVKLT LPTCFTSILT GPSVNGSTVR MGEYSSGTIK NGASPVPFDI SLQNCIRVRN IETKLVTGKV GTQNTQLLGN TLTGSTAAKG VGVLIEGLAT SKNPLMTLKP NDTNSVYIDY ETEDDTSDGV YPNQGNGTSQ PLHFQATLKQ DGNIAIEPGE FKATSTFQVT YP	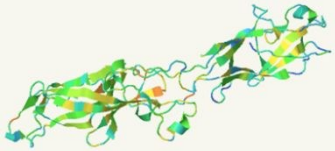	Amino acids : 412 Total charge : 0 Mw : 52253 g/mol Length : 13.1 nm
YadN	MSKKLGFALS GLMLAMVAGT ASADMDGGQL NISGLVVDNT CETRVDGGNK DGLILLQTAT VGEIDAGVLN DTVGAKAKPF SITVDCSKAN PNPGSTAKMT FGSVFFGNSK GTLNNDMSIN NPSDGVNIAL HNIDGSTIKQ VQINNPGDVY TKALDATTKS AVYDFKASYV RAVADQTATA GYVKTNTAYT ITYQ	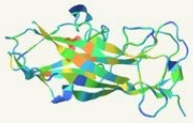	Amino acids : 194 Total charge : - 1 Mw : 23573 g/mol Length : 7.8 nm
FimA	MKIKTLAIVV LSALSLSSTA ALAAATTVNG GTVHFKGEVV NAACAVDAGS VDQTVQLGQV RTASLAQEGA TSSAVGFNIQ LNDCDTNVAS KAAVAFLGTA IDAGHTNVLA LQSSAAGSAT NVGVQILDRT GAALTLDGAT FSSETTLNNG TNTIPFQARY FATGAATPGA ANADATFKVQ YQ	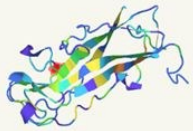	Amino acids : 182 Total charge : - 1 Mw : 21356 g/mol Length : 7.2 nm
FimH	MKRVITLFAV LLMGWSVNAW SFACKTANGT AIPIGGGSAN VYVNLAPVVN VGQNLVVDLS TQIFCHNDYP ETITDYVTLQ RGSAYGGVLS NFSGTVKYSG SSYPFPTTSE TPRVVYNSRT DKPWPVALYL TPVSSAGGVA IKAGSLIAVL ILRQTNNYNS DDFQFVWNIY ANNDVVVPTG GCDVSARDVT VTLPDYPGSV PIPLTVYCAK SQNLGYYLSG TTADAGNSIF TNTASFSPAQ GVGVQLTRNG TIIPANNTVS LGAVGTSAVS LGLTANYART GGQVTAGNVQ SIIGVTFVYQ	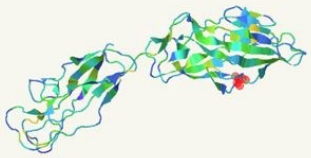	Amino acids : 300 Total charge : +2 Mw : 36829 g/mol Length : 12.3 nm

View Article Online
DOI: 10.1039/D0NR06840C

Figure captions

Figure 1. Images of *E. coli* Δ_4*adh*_PcL*yad* cells and Yad fimbriae recorded by AFM operated in PeakForce Tapping mode under air conditions at 23°C (scan rate: 0.95 Hz, samples/line: 512, Peak Force setpoint: 0.876 nN, Peak Force amplitude: 120 nm, PFT Gain: 6). (a), (b) a single bacterium; (c), (d) identification of several Yad fimbriae with their corresponding height profile (e) and (f), respectively. The white squares in (b) define the zoom regions given in (c) and (d).

Figure 2. Adhesion (a) and surface coverage (b) of *E. coli* Δ_4*adh* and Δ_4*adh*_PcL*yad* cells after 2 hours incubation onto several SAMs-coated gold substrates covered by YadC, YadN antibodies, xylose (Xyl), galactose (Gal), lactose (Lac), mannose (Man), or with –OH, $–CH_3$, $–NH_2$ and –COOH terminated alkanethiols. ANOVA test was used to compare the differences in the median adhesion values for *E. coli* Δ_4*adh* and Δ_4*adh*_PcL*yad;* there is a statistically significant difference for * p value < 0.050 (no difference for p value > 0.1).

Figure 3. Illustrative force *vs.* separation distance profiles (black circles) measured by SMFS upon withdrawal of several AFM-probes (functionalized with anti-YadC, anti-YadN antibodies, xylose (Xyl), galactose (Gal), lactose (Lac) and mannose (Man)) from cell wall of *E. coli* Δ_4*adh*_PcL*yad*. Red lines correspond to theoretical fitting on the basis of the Worm-Like-Chain model (eq 1).

Figure 4. Statistic distribution of the adhesion forces between *E. coli* Δ_4*adh*_PcL*yad* cells and the different AFM-probes functionalized with anti-YadC, anti-YadN antibodies, xylose (Xyl), galactose (Gal), lactose (Lac) and mannose (Man) (indicated). Red lines correspond to decomposition of the distribution into fundamental Gaussian components.

View Article Online
DOI: 10.1039/D0NR06840C

Figure 5. Statistic distribution of the maximal rupture distances (or maximal Yad fimbriae elongation prior to rupture) estimated from the SMFS force-distance curves measured for *E. coli* Δ_4*adh*_PcL*yad* cells interacting with AFM-probes functionalized with anti-YadC, anti-YadN antibodies, xylose (Xyl), galactose (Gal), lactose (Lac) and mannose (Man) (indicated). Red lines correspond to decomposition of the distribution into fundamental Gaussian components.

Figure 6. Statistic distribution of the distance between two successive adhesive events detected on the SMFS force-curves collected for *E. coli* Δ_4*adh*_PcL*yad* cells in interaction with AFM-probes functionalized with anti-YadC, anti-YadN antibodies, xylose (Xyl), galactose (Gal), lactose (Lac) and mannose (Man) (indicated).

Figure 7. Schematics for the structure of Yad fimbriae and its possible conformation during stretching by antibodies or xylose residues grafted at the apex of AFM probes.

Figure 8. Dependence of the surface concentration of bacteria adhered onto SAMs-coated gold substrates covered by anti-YadC, anti-YadN antibodies, xylose (Xyl), galactose (Gal), lactose (Lac), mannose (Man) on their corresponding median adhesive interactions measured between AFM-probes functionalized with anti-YadC, anti-YadN antibodies, xylose (Xyl), galactose (Gal), lactose (Lac) and mannose (Man) (specified in the figure) and individual *E. coli* Δ_4*adh*_PcL*yad* cells. Dashed line corresponds to linear fitting of the data in semi-logarithmic scale.

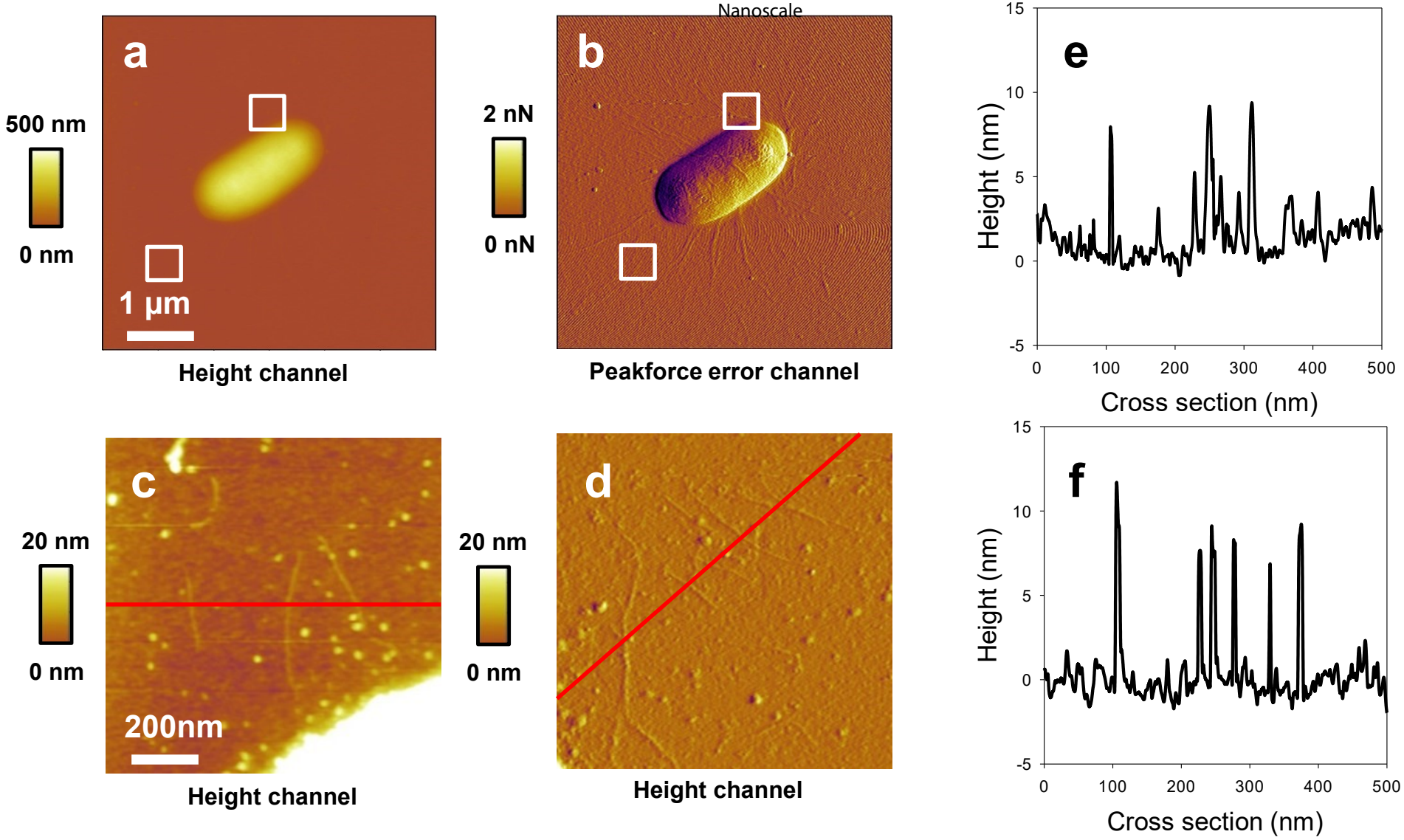

Figure 1 : Figure 1. Images of *E. coli* Δ*4adh*_PcL*yad* cells and Yad fimbriae recorded by AFM operated in PeakForce Tapping mode under air conditions at 23°C (scan rate: 0.95 Hz, samples/line: 512, Peak Force setpoint: 0.876 nN, Peak Force amplitude: 120 nm, PFT Gain: 6). (a), (b) a single bacterium; (c), (d) identification of several Yad fimbriae with their corresponding height profile (e) and (f), respectively. The white squares in (b) define the zoom regions given in (c) and (d).

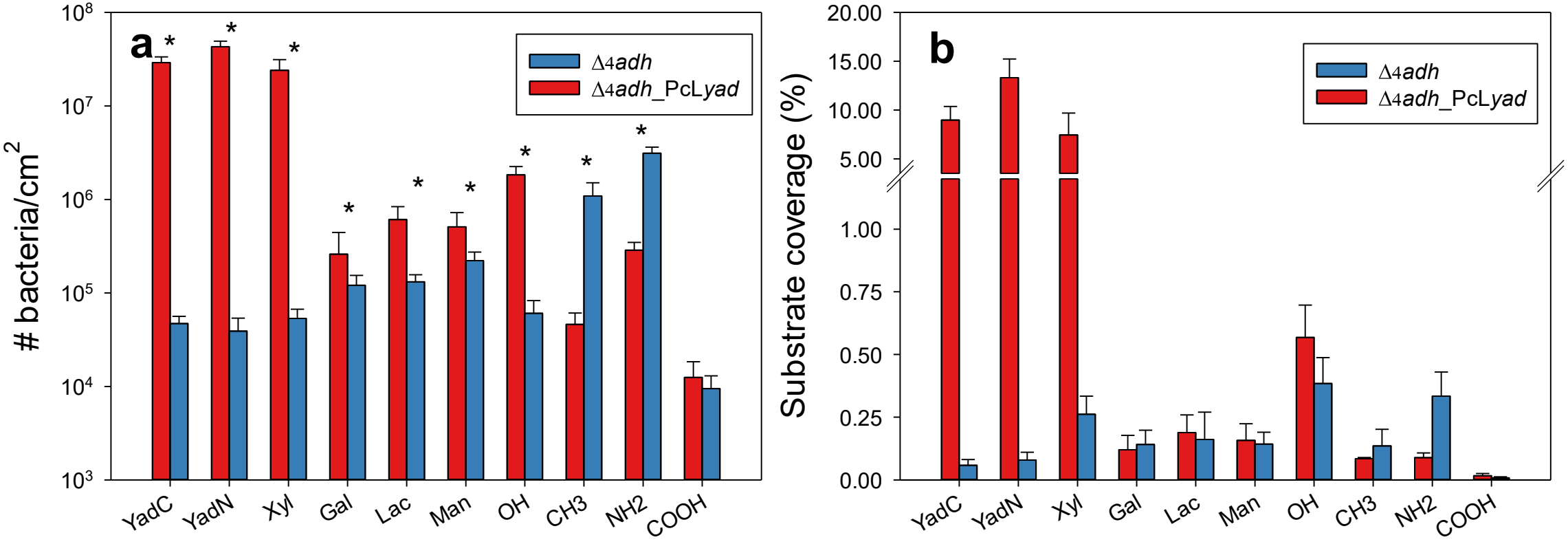

Figure 2 : Adhesion (a) and surface coverage (b) of *E. coli* Δ_4*adh*_PcL*yad* and Δ_4*adh* after 2 hours incubation onto several SAMs-coated gold substrates covered by YadC, YadN antibodies, xylose (Xyl), galactose (Gal), lactose (Lac), mannose (Man), or with –OH, –CH3, –NH2 and –COOH terminated alkanethiols. ANOVA test was used to compare the differences in the median adhesion values for *E. coli* Δ_4*adh*_PcL*yad* and Δ_4*adh*; there is a statistically significant difference for * p value < 0.050 (no differences for p value > 0.100).

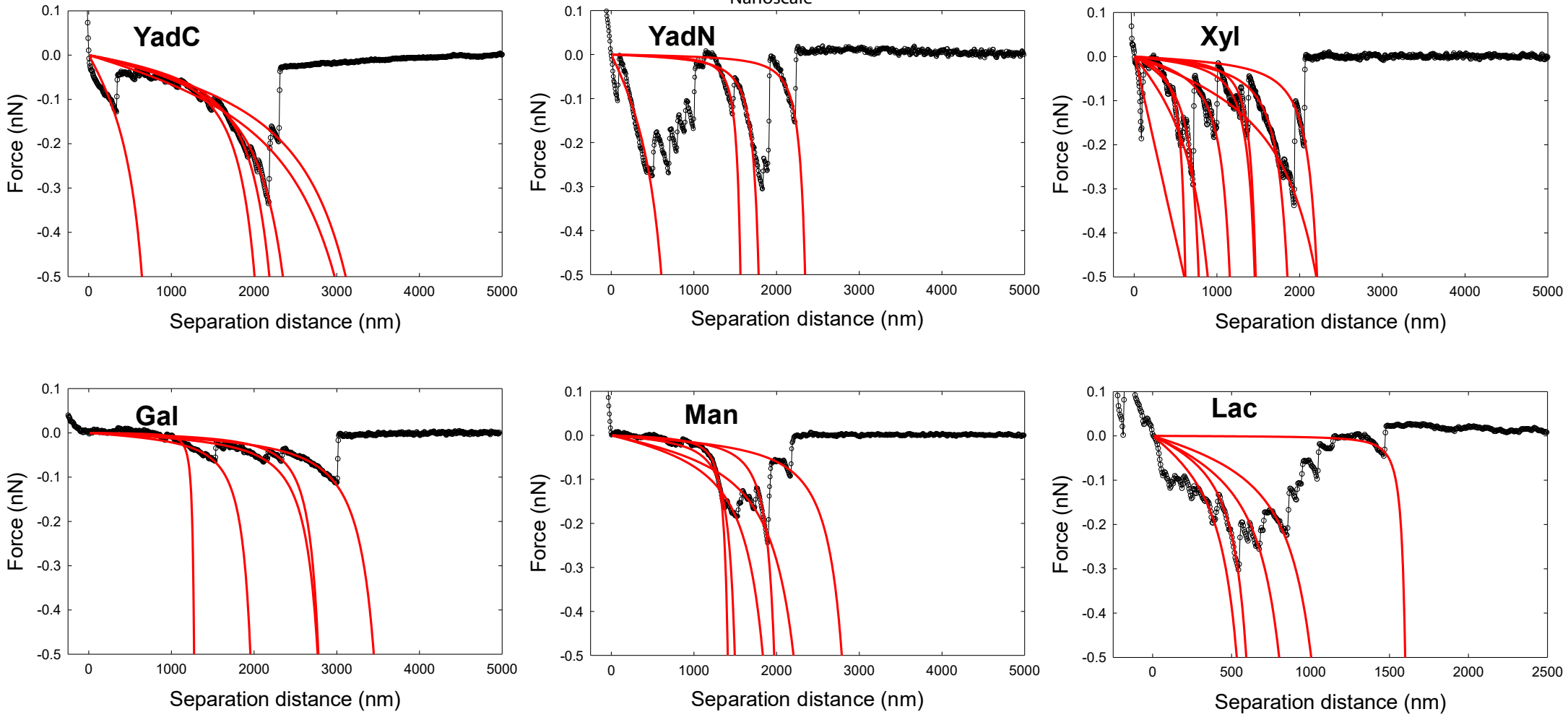

Figure 3 : Illustrative force vs. separation distance profiles (black circles) measured by SMFS upon withdrawal of several AFM-probes (functionalized with YadC, YadN antibodies, xylose (Xyl), galactose (Gal), lactose (Lac) and mannose (Man)) from the cell wall of *E. coli* Δ_4*adh*_PcL*yad*. Red lines correspond to theoretical fitting on the basis of the Worm-Like-Chain model (eq 1).

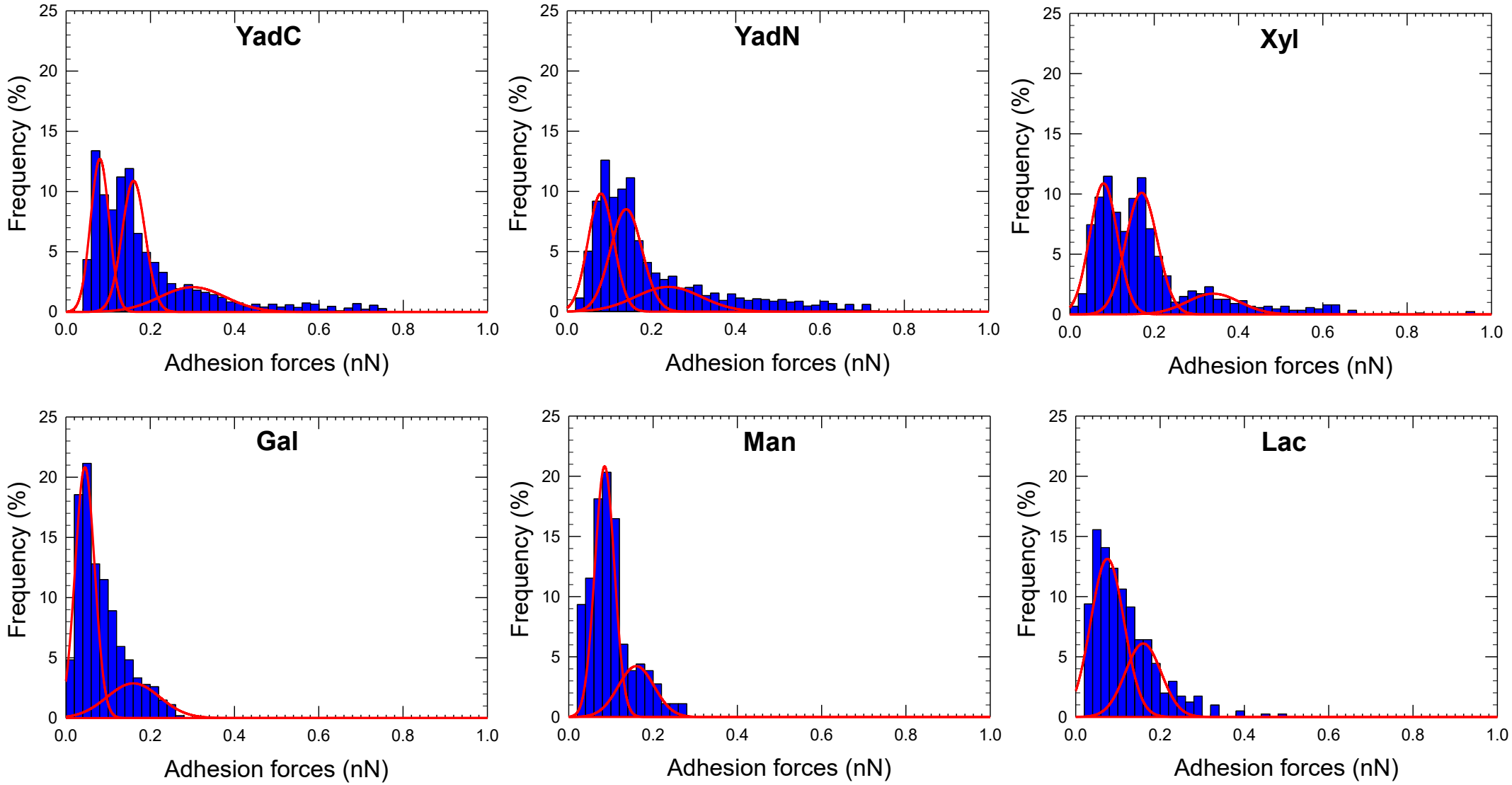

Figure 4 : Statistic distribution of the adhesion forces between *E. coli* Δ_4*adh*_PcL*yad* and the different AFM-probes functionalized with YadC, YadN antibodies, xylose (Xyl), galactose (Gal), lactose (Lac) and mannose (Man) (indicated). Red lines correspond to decomposition of the distribution into fundamental Gaussian components.

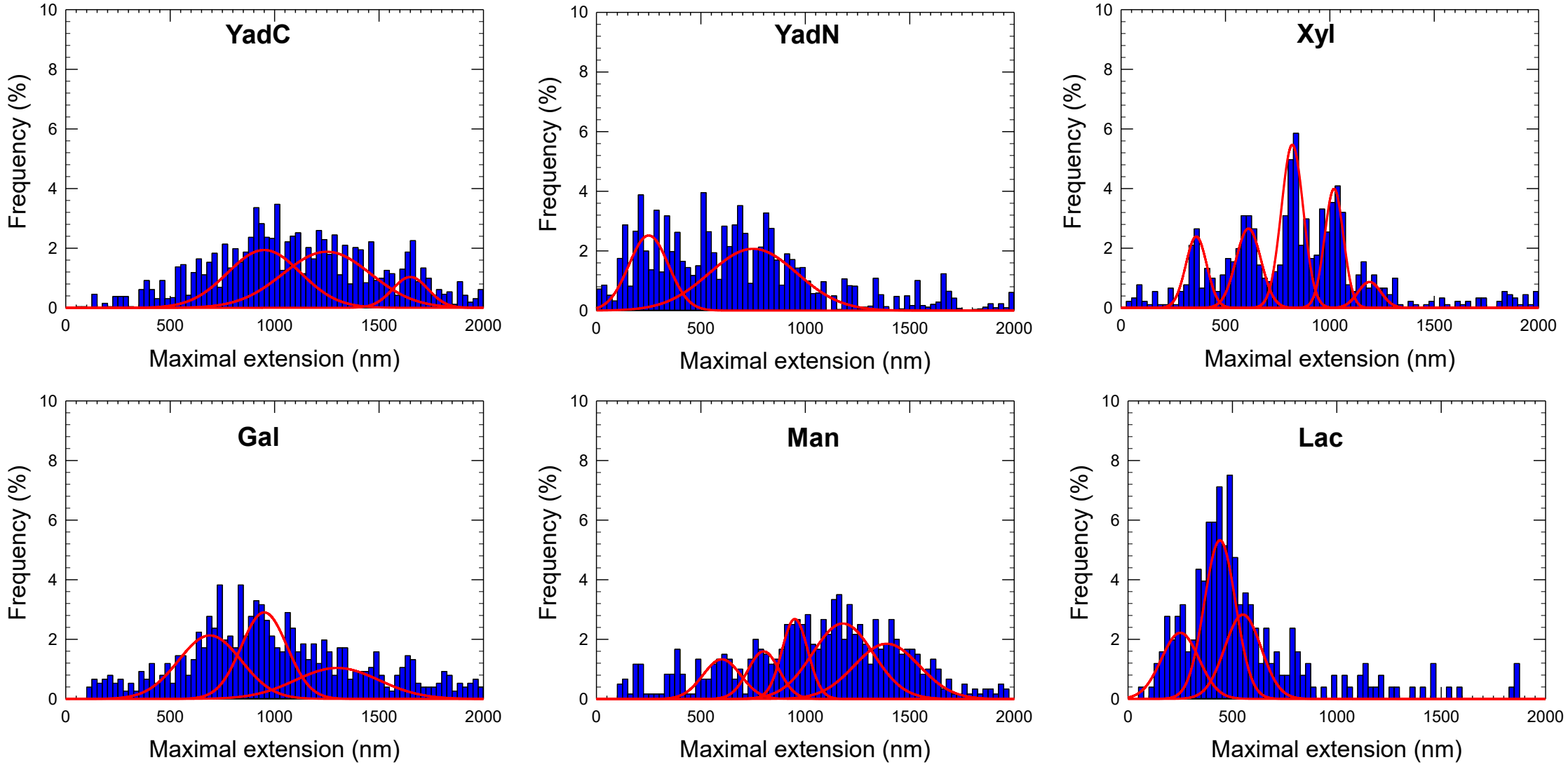

Figure 5 : Statistic distribution of the maximal rupture distances (or maximal Yad fimbriae elongation prior to rupture) estimated from the SMFS force-distance curves measured for *E. coli* Δ_4*adh*_PcL*yad* interacting with AFM-probes functionalized with YadC, YadN antibodies, xylose (Xyl), galactose (Gal), lactose (Lac) and mannose (Man) (indicated). Red lines correspond to decomposition of the distribution into fundamental Gaussian components.

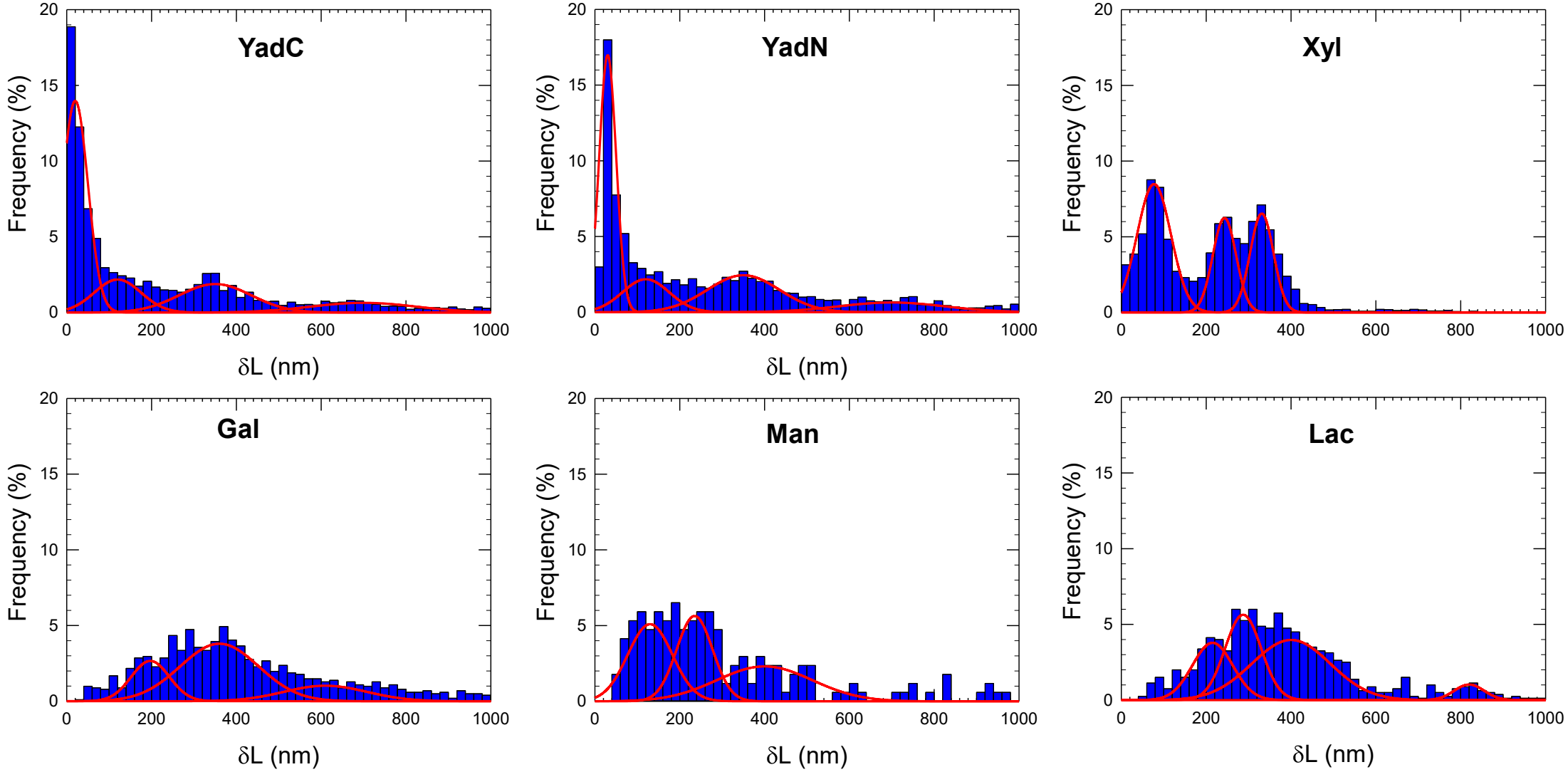

Figure 6 : Statistic distribution of the distance between two successive adhesive events detected on the SMFS force-curves collected for *E. coli* Δ_4*adh*_PcL*yad* in interaction with AFM-probes functionalized with YadC, YadN antibodies, xylose (Xyl), galactose (Gal), lactose (Lac) and mannose (Man) (indicated).

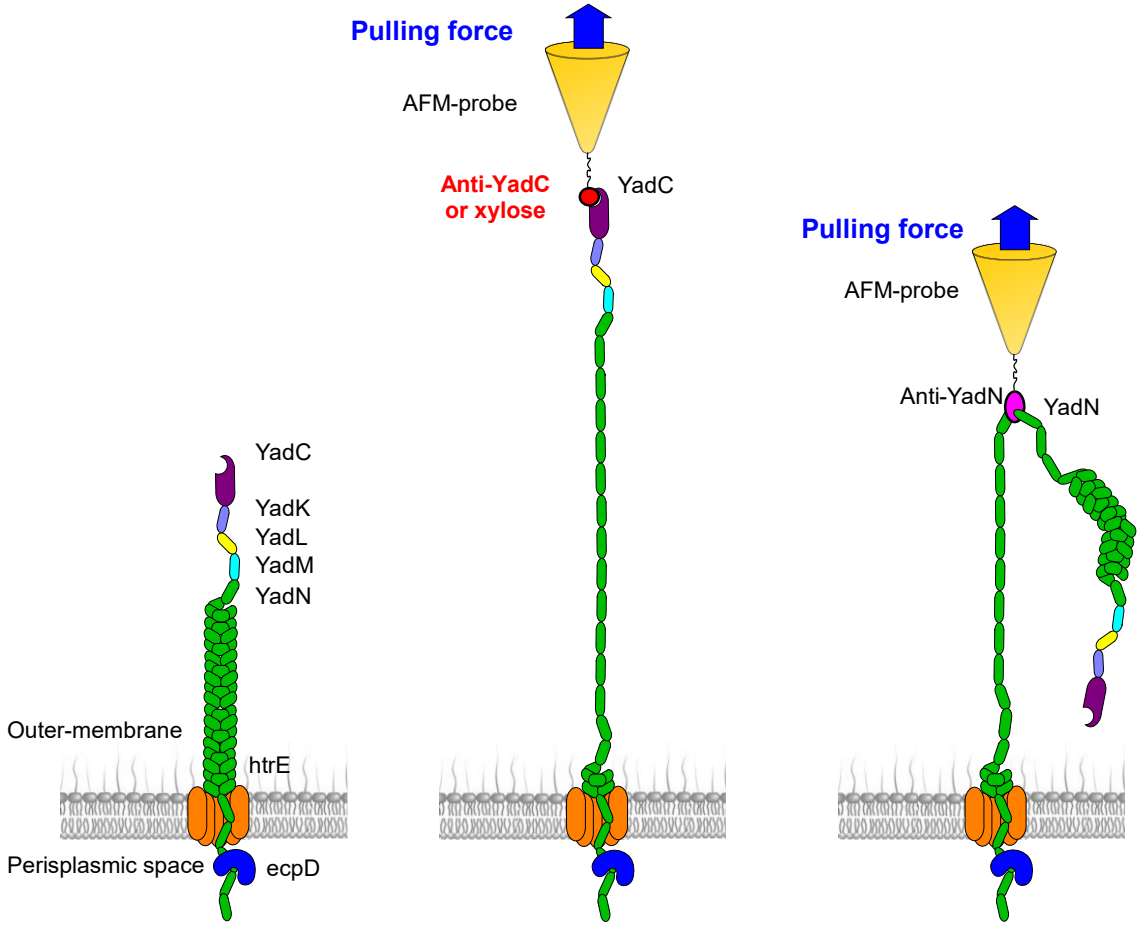

Figure 7 : Schematics for the structure of Yad fimbriae and its possible conformation during stretching by antibodies or xylose residues grafted at the apex of AFM probes.

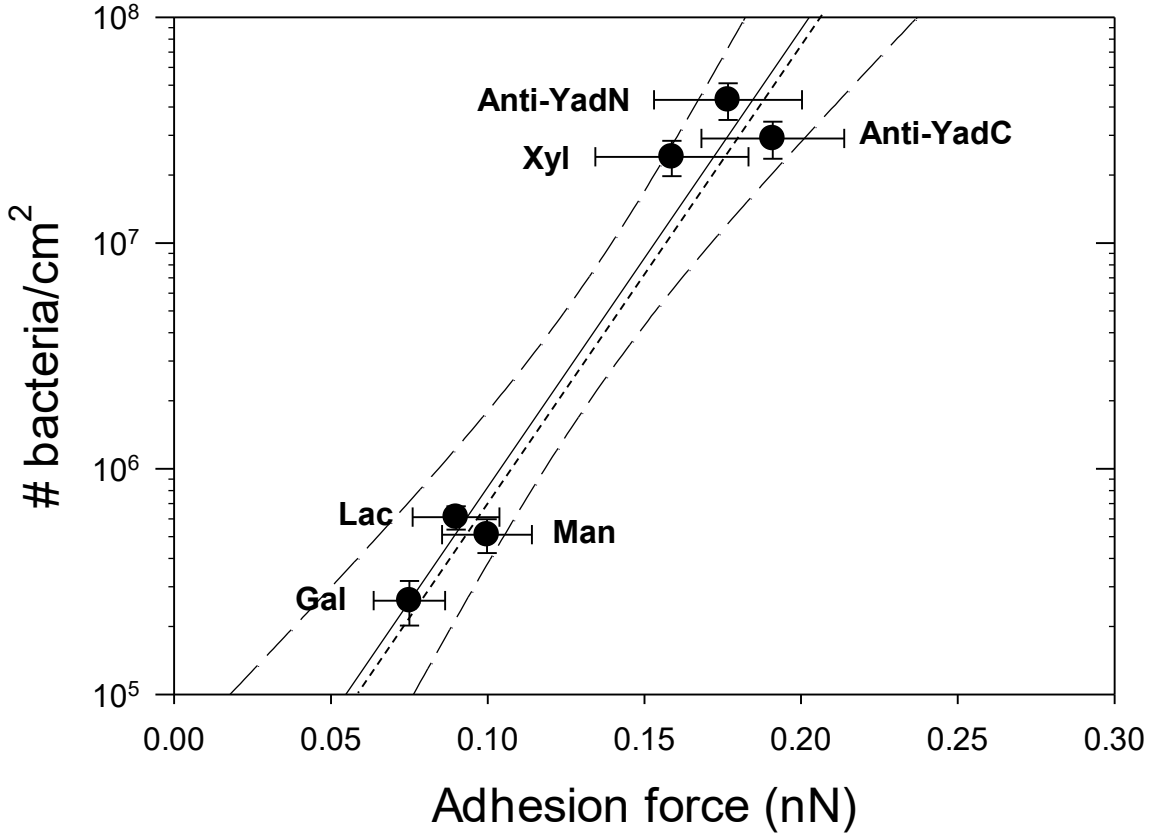

Figure 8 : Dependence of the surface concentration of bacteria adhered onto SAMs-coated gold substrates covered by YadC, YadN antibodies, xylose (Xyl), galactose (Gal), lactose (Lac), mannose (Man) on their corresponding adhesive interactions measured between AFM-probes functionalized with YadC, YadN antibodies, xylose (Xyl), galactose (Gal), lactose (Lac) and mannose (Man)) and individual *E. coli* Δ_4*adh*_PcL*yad*. Dashed line corresponds to linear fitting of the data in semi-logarithmic scale.